Winter Spring Summer Autumn

SWECLIM regional
modeling domain

0.0 0.8 1.6 2.4 3.2 4.0 4.8 0.0 0.8 1.6 2.4 3.2 4.0 4.8 0.0 0.8 1.6 2.4 3.2 4.0 4.8 0.0 0.8 1.6 2.4 3.2 4.0 4.8

Sea surface temperature change

The first Rossby Centre regional climate scenario for the Baltic Sea using a 3D coupled ice-ocean model

H.E. Markus Meier
Rossby Centre

The first Rossby Centre regional climate scenario for the Baltic Sea using a 3D coupled ice-ocean model

H.E. Markus Meier
Rossby Centre

Report Summary / Rapportsammanfattning

Title (and Subtitle/Titel
The first Rossby Centre regional climate scenario for the Baltic Sea using a 3D coupled ice-ocean model.

Abstract/Sammandrag

Temperature, salinity, sea ice and sea level in the Baltic Sea have been analyzed under different climate conditions using a 3D coupled ice-ocean model. As a reference, hindcast simulations for the period 1980-93 have been performed with observed three-hourly meteorological forcing fields and observed monthly river runoff. The observed Baltic Sea climate is well reproduced by the model. Furthermore, two sets of 9-year time slice experiments have been performed using results of an atmospheric regional climate model as forcing, one representing pre-industrial climate conditions (control simulation), and the other one global warming with a 150% increase of CO_2 greenhouse gas concentration (scenario simulation). At the boundaries of the regional climate model results of the global atmosphere-ocean general circulation model HadCM2 (Hadley Centre) have been prescribed. To simulate river runoff, a large-scale hydrological model has been applied. As the time slices are too short to spin up initial stratification for future climate, salinity is treated as uncertainty. An extreme condition is obtained, integrating the Baltic Sea model for 100 years assuming that no salt water inflow occurs in future. The area averaged annual mean sea surface temperature change between scenario and control run is about 2.3°C. Seasonal variability of the change is small compared to the corresponding 2 m air temperature change. The uncertainty due to unknown future initial conditions is relatively small (largest in summer with -0.5°C). The decrease of mean ice extent in the scenario compared to the control run is dramatic, from $210 \cdot 10^9 m^2$ to $82 \cdot 10^9 m^2$ (a relative change of 61%). However, in all years ice can still be found in the Bothnian Bay. The minimum ice extent is $16 \cdot 10^9 m^2$ (for comparison: the area of the Bothnian Bay is about twice as large). The mean number of ice days decreases significantly, too. In the fast ice zone of the Bothnian Bay (Kemi) the mean ice season becomes 40 days shorter. The ice in the scenario run is thinner with less snow on top. In the central Bothnian Bay mean maximum annual ice thickness is reduced by 25 cm from 54 to 29 cm. Model dependent uncertainties are discussed.

Key words/sök-, nyckelord
Baltic Sea, climate change, dynamical downscaling, regional climate modelling, spin-up problem

Contents

1 Introduction

At present, in several institutes around the world global coupled atmosphere-ocean general circulation models (OAGCMs) are used to predict greenhouse gas induced anthropogenic climate changes in future. Unfortunately, these models are still too coarse to resolve regional scales of interest for climate change impact studies. One of the several techniques being used to forecast climate changes on the regional scale is dynamical downscaling. In this approach, a high-resolution limited-area model is run with boundary data taken from a GCM simulation.

Recently, regional climate simulations for an area covering northern and central Europe have been conducted at the Rossby Centre within the SWEdish regional CLImate Modelling program, SWECLIM (see Rummukainen et al. 2000; Räisänen et al. 2000). The model used is the Rossby Centre regional climate Atmosphere model (RCA). SWECLIM aims to increase our knowledge of effects of climate change in Sweden and the other Nordic countries. Specific regional consequences of global climate change like river discharge, precipitation, ice cover, air and sea temperatures and water quality conditions are of special interest for the Nordic societies. The oceanographic and sea ice modeling activities within SWECLIM aim to simulate and to understand long-term changes and natural variability of the Baltic Sea. For that purpose, the Rossby Centre regional Ocean climate model (RCO) has been developed, a 3D coupled ice-ocean model for the Baltic Sea (Meier et al. 1999).

In this report, dynamical downscaling results of RCA with boundary data from an OAGCM, HadCM2 (Johns et al. 1997), have been used as atmospheric forcing for RCO to regionalize climate change in the Baltic Sea. Two 9-year time slice simulations representing control (pre-industrial) and scenario (future) climate are performed and analyzed.

Scenarios for ice conditions in the Baltic Sea have been performed earlier by Haapala and Leppäranta (1997). They used the coupled ice-ocean model of Haapala and Leppäranta (1996) to forecast ice conditions in 2050. In a new version of this model, the ice thickness re-distribution is based on physical ice classes. The pack ice is decomposed to open water, to level and lead ice, and to rafted, rubble and ridged ice (Haapala 2000). The ice model is coupled to a simplified ocean model, in which ocean surface currents are approximated by vertical averaged velocities and freshwater fluxes (runoff and net precipitation) are neglected. Based on the multi-ice-class approach, Haapala et al. (2000) have performed control and scenario simulations using the same forcing data of RCA as used in this study.

Omstedt et al. (2000) investigated the water and heat balance in GCM and regional climate models using the basin wide integrated, process oriented PROBE-Baltic model (Omstedt 1990). Omstedt's model consists of 13 boxes with high vertical resolution using parameterizations for horizontal transports between the boxes. Their results are obtained using downscaling simulations of an earlier RCA version (RCA0).

1

Also for some other shelf seas the technique of dynamical downscaling has been applied to regionalize scenario simulations of GCMs. For example, a regional version of the OGCM OPYC for the North Sea with open boundaries and tides have been used by Kauker (1998) for dynamical downscaling from the OAGCM ECHAM4/OPYC3 (Roeckner et al. 1996).

The report is organized as follows:

In the second section an overview of natural variability and long-term changes of the Baltic Sea estuary is presented. In the third section the coupled ice-ocean model is described briefly. The numerical experiments performed for this study are summarized in Section 4. Due to the time slice approach, the problem occurs, how to spin up initial conditions for the scenario run. This is discussed in Section 5. The results of hindcast, control and scenario runs are presented in Section 6. The report ends with discussion and conclusions.

2   Background

The Baltic Sea is the world's largest brackish water sea area with a total surface, excluding the Danish Sounds, of 377,400 km² and a corresponding volume of 21,200 km³ (Sjöberg 1992). The mean water depth amounts to 56 m and the maximum depth to 451 m (Landsort Deep). The highly variable bottom topography separates the water masses into separate basins, delimited by high sills, or bays (Fig.1). These are, listed from North to South, Bothnian Bay, Bothnian Sea, Åland Sea, Archipelago Sea, Gulf of Finland, Gulf of Riga, Northwestern and Eastern Gotland Basin, Bornholm Basin and Arkona Basin (cf. Fig.1). Important channels or sills of the inner Baltic are the Quark separating Bothnian Bay and Bothnian Sea (sill depth of about 20 m), the Southern Quark separating Bothnian Sea and Baltic proper (40 m), the Irba Strait separating Gulf of Riga and Baltic proper (21 m), Stolpe or Slupsk Channel separating Gotland and Bornholm Basin (sill depth of 60 m) and Bornholm Channel separating Bornholm and Arkona Basin (40 m).

The water exchange between Baltic and North Sea is restricted by the narrows and sills of the Danish Straits. The width of the narrowest part of the Sound, near Helsingør-Helsingborg, amounts to approximately 4 km. Darss Sill, having a depth of about 18 m, separates the Belt Sea from the Arkona Basin. The Sound has a sill depth of only 8 m at its southern entrance at Drogden.

The mean annual river discharge to the Baltic Sea is 15,310 m³ s⁻¹ for the period 1950-1990 (Bergström and Carlsson 1994). This inflow originates from the huge drainage basin with a size of 1,729,000 km². The river flow is highly variable over the year and there are large inter-annual variations. The lowest (11,132 m³ s⁻¹ in 1976) and highest (18,660 m³ s⁻¹ in 1981) annual values differ from the mean value by -27% and $+22\%$, respectively, for the period 1950-1990. The maximum recorded monthly average con-
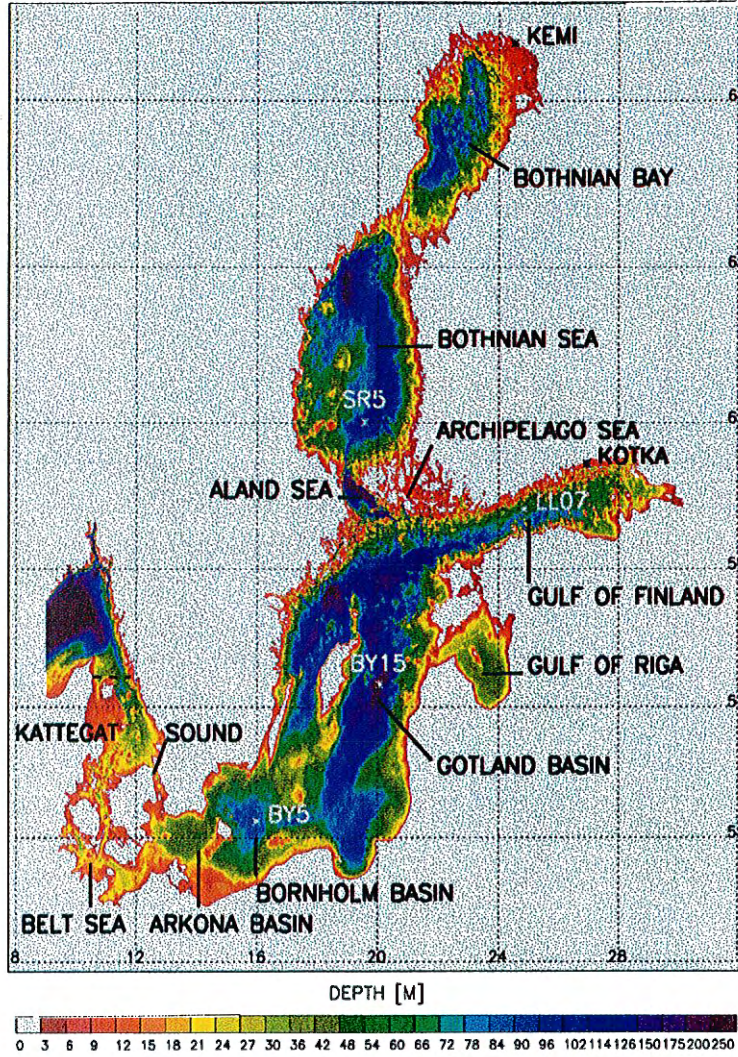
2

Figure 1: *Bottom topography of the Baltic Sea including Kattegat and Skagerrak (data from Seifert and Kayser, 1995). The model domain of RCO is limited with open boundaries in the northern Kattegat (dashed line).*

tribution occurred was 32,411 m^3 s^{-1} in May 1966 and the lowest was 7,635 m^3 s^{-1} in December 1959. Surface freshwater fluxes (i.e., precipitation minus evaporation) are less important. For the period 1981-1994, Omstedt et al. (1997) calculated the total mean atmospheric freshwater inflow to be 1,986 m^3 s^{-1}.

A pronounced feature of the Baltic is the seasonal sea ice cover. Sea ice acts as a relatively rigid insulating film between the air and the sea, which modifies air-sea exchange of momentum, heat and material and influences local meteorological conditions. With respect to the ocean, sea ice influences the temperature and salinity characteristics of the water masses and the circulation of the Baltic Sea. Normally, the ice season lasts 5-7 months, from November to May, with large inter-annual variability of ice ex-

3

tent. During a mild winter ice occurs only in the Bothnian Bay, but in a severe winter the entire Baltic Sea becomes ice-covered (see SMHI and FIMR 1982). As surface albedo changes drastically with ice conditions, sea ice in the Baltic is regarded as a key element in the North-European climate system. In addition, Baltic sea ice is a good indicator for climate change, because ice extent and mean winter temperature in North and Central Europe are strongly correlated (e.g. Tinz 1996). Natural variability of ice cover is related to the large scale circulation. As shown by Koslowski and Loewe (1994) variability of the western Baltic sea ice season in terms of a mass-related severity index is governed by the North Atlantic Oscillation (NAO). A review of long-term ice observations is given by Haapala and Leppäranta (1997).

The restricted water exchange through the Danish Straits and the river runoff into the Baltic Sea determine the stratification of the water masses into a homogeneous upper layer and a stratified lower layer. In the pioneering work of Knudsen (1899, 1900) the steady state water exchange was described as two-layer flow with outflow in the upper and inflow in the lower layer, respectively. Transient states of this two-layer fjord-type estuary, in case of small perturbations, are discussed by Welander (1974) analytically.

However, during the past 100 years Baltic Sea stratification and ventilation of the bottom water in deep sub-basins are affected mainly by large perturbations, so-called major Baltic salt water inflows (Matthäus and Franck 1992). These events occur randomly during winter season at intervals from one to several years. Major salt water inflows are very likely forced by a sequence of easterly winds in late autumn, lasting for 20-30 days, followed by strong to very strong westerly winds of similar duration (Lass and Matthäus 1996). Matthäus and Schinke (1994) discussed mean large scale atmospheric circulation patterns associated with major Baltic inflows between 1899 and 1976. About two weeks before the start of the main inflow period, the Azores High shifts to north-east and its pressure increases. At the same time, the center of lowest pressure moves eastward from the Greenland-Icelandic area to northern Norway, strengthening as it moves. Due to these movements, very strong pressure gradients occur over the North Sea and the entrance area to the Baltic. Matthäus and Schinke (1994) found the maximum gradients two days before and on the first day of the main inflow event, respectively.

Since the mid-1970s the frequency and intensity of major inflows decreases and were completely absent from February 1983 to the beginning of 1993. During this phase a significant loss of salt in the deep layer of the Gotland Basin with a simultaneously depletion of oxygen and increase of hydrogen sulphide was observed. A major salt water inflow in January 1993 terminated this exceptionally long stagnation period (Matthäus and Lass 1995). Despite of the unusual climate conditions, the period 1980-1993 has been selected in this study for hindcast integrations, because homogeneous observational data sets for atmospheric variables and river runoff with sufficient quality, to force a 3D Baltic Sea model, are available.

To explain the decreased frequency of major inflows, two mechanisms are discussed in the literature. Lass and Matthäus (1996) argued, that the lack of major inflows was

4

due to changes in the wind field over the North Sea and the Baltic compared to the time interval before. Schinke and Matthäus (1998) and Matthäus and Schinke (1999) found that variations in river runoff have a greater impact on the occurrence of major inflows than hitherto supposed. They concluded, that increased zonal circulation might result in intensified precipitation in the Baltic region and increased river runoff. In addition, river regulation re-distributes runoff over many months and gives rise to higher values during autumn and winter. Increased winter runoff (averaged from September to March) seems to reduce the probability of major Baltic inflows. It is noteworthy, that these changes coincidence with changes in large scale circulation patterns. A recent study on the link between the North Atlantic Oscillation (NAO) and the Arctic ice export (Hilmer and Jung 2000) revealed an eastward shift in the position of the NAO centers of inter-annual variability during the two last decades. However, further investigations in this field are still necessary to elucidate involved processes.

A history of long-term Baltic Sea modeling is summarized by Omstedt et al. (2000).

3 The coupled ice-ocean model

RCO is a further development of the OCCAM version (Ocean Circulation Climate Advanced Modeling Project at the James Rennel Division, Southampton Oceanography Centre, Southampton, UK; see Webb et al. 1997) of the widely used Bryan–Cox–Semtner primitive equation ocean model (Bryan 1969; Semtner 1974; Cox 1984) with a free surface (Killworth et al. 1991). OCCAM includes improved vertical and horizontal advection schemes (Webb 1995; Webb et al. 1998), harmonic horizontal viscosity and diffusivity and a third order polynomial approximation (Bryan and Cox 1972) for the equation of state, as proposed by the Joint Panel on Oceanographic Tables and Standards (UNESCO 1981) and as described by Gill (1982). The conservation equations of momentum, mass, potential temperature and salinity are discretized in spherical co-ordinates on the Arakawa–B–grid (Mesinger and Arakawa 1976) horizontally and in geopotential levels vertically.

The model domain of RCO is limited with open boundaries in the northern Kattegat (see Fig.1). Open boundary conditions, as developed by Stevens (1990, 1991), are utilized.

The model depths are based on realistic bottom topography data (Seifert and Kayser 1995; Fig.1). RCO makes use of 41 levels with layer thicknesses from 3 m close to the surface to 12 m near the bottom. The maximum depth in RCO is only 250 m, to avoid small time steps. The horizontal resolution is 6 nm, corresponding to $\Delta\varphi = 6'$, $\Delta\lambda = 12'$ with latitude φ and longitude λ.

As mixing plays a dominant role for the physics of an estuary like the Baltic Sea, a sophisticated two-equation turbulence model of the $k - \epsilon$ type (cf. Svensson 1979; Rodi 1980; Omstedt et al. 1983) is used with corrected dissipation term, flux boundary

conditions to include the effect of a turbulence enhanced layer due to breaking surface gravity waves and a parameterization for breaking internal waves (Meier 2000).

The ocean model in RCO is coupled with a Hibler-type (Hibler 1979) two-level (open water and ice) dynamic-thermodynamic sea ice model. An extension of the widely used viscous-plastic rheology with an elastic component (Hunke and Dukowicz 1997) leads to a fully explicit numerical scheme, that improves computational efficiency, particularly on high resolution grids, and easily adapts to parallel computer architectures. Within each time step, the dynamic component needs to be sub-cycled several times to damp elastic waves. As described in Hunke and Zhang (1999), the elastic term initially makes a prediction for the ice stress, which is then 'corrected' towards the viscous-plastic solution by means of sub-cycling. By choosing the number of sub-cycles (N), a compromise has to be made between an energetic solution, that quickly adjusts during rapidly changing forcing conditions (small N), and a solution, that does not significantly differ from the viscous-plastic one on longer time scales (high N). The model sensitivity on artificial, rheology specific parameters and on horizontal resolution is quite small, showing the robustness of the method. The equations of the ice model are discretized on the same grid as used for the ocean.

The ice thermodynamic is based on Semtner's layer models (Semtner 1976) for thick ice/snow (multiple layers) and thin ice/snow ('zero'-layer) using characteristic discrimination thicknesses for ice (25 cm) and snow (15 cm). In RCO thick ice consists of one or two layers and thick snow consists of one layer. The reason for the discrimination between thick and thin ice/snow is numerical stability. The 'zero'-layer models for ice and snow are based on simple heat budgets. Precipitation from the atmosphere model over sea ice is assumed to be converted to snow. Snow is converted to snow ice, if flooding (as calculated from Archimedes' law) occurs.

Standard bulk formulae are used to calculate sea surface wind stress, sensible and latent heat fluxes, shortwave and longwave radiation, see Appendices A and B. The albedo for the open water surface is calculated from Fresnel's formula. In case of ice, four different surface albedos for dry and wet ice and for dry and wet snow are employed according to Perovich (1996).

For a more detailed model description of RCO, the reader is referred to Meier et al. (1999), Meier (2000) and Meier et al. (2001). Results of 13-year hindcast simulations for the period May 1980 until December 1993 have been compared with observations by Meier (1999). A performance analysis of the multiprocessor model is given by Meier and Faxén (2001).

4   Numerical experiments

In Table 1 the experiments performed for this study are summarized. They are divided into three groups: hindcast, control and scenario runs. Sensitivity experiments within

#	Experiment	RCO version	Meteorological forcing	River runoff	Sea level Kattegat	Integration length
H1	hindcast (standard)	RCO-a	SMHI database	observed	1980-93	13.6 yr
H2	hindcast	RCO-a	ERA wind, SMHI database	observed	1980-93	13.6 yr
H3	hindcast	RCO-b	SMHI database	observed	1980-93	13.6 yr
H4	hindcast	RCO-a, $S = 0$	SMHI database	observed	1980-93	13.6 yr
H5	hindcast	RCO-a, Ri mix	SMHI database	observed	1980-93	13.6 yr
C1	control (standard)	RCO-a	RCA1 control	HBV control	1980-89	9.5 yr
C2	control	RCO-a	SMHI database	HBV control	1980-89	10.0 yr
C3	control	RCO-b	RCA1 control	HBV control	1980-89	9.5 yr
S1	scenario (standard)	RCO-a	RCA1 scenario	HBV scenario	1980-89	9.5 yr
S2	scenario	RCO-a	RCA1 scenario sub-cycling	HBV hindcast plus change	1980-89 sub-cycling	99.5 yr
S3	scenario	RCO-b	RCA1 scenario	HBV scenario	1980-89	9.5 yr
S4	scenario	RCO-a, $S = 0$	RCA1 scenario	HBV scenario	1980-89	9.5 yr
S5	scenario	RCO-a	RCA1 scenario	HBV scenario	1980-89 + 50 cm	9.5 yr

Table 1: *Experiments performed for this study using the Baltic Sea coupled ice-ocean model, RCO. RCO-a and RCO-b denote two versions with different radiative surface heat fluxes (see Tab.2). In experiments H4 and S4 salinity is kept equal to zero and in experiment H5 Richardson number dependent friction is used. RCA1 is the revised version of the Rossby Centre regional climate atmosphere model with 88 km horizontal resolution and with boundary data from the global HadCM2 simulations. HBV-Baltic is a regional river runoff model for the Baltic Sea catchment area. The atmospheric forcing in case of the hindcast experiments consists of three hourly horizontal maps of surface variables based on observations (SMHI database) or six hourly re-analysis wind fields. In all experiments (hindcast, control or scenario runs), observed initial conditions for May 26 1980 and hourly sea level observations from the Swedish tide gauge Ringhals in Kattegat (57°N 15′, 12°E 5′) are used. In experiment S5 an assumed global mean sea level rise of 50 cm is added to these sea level data. In case of inflow, temperature and salinity are nudged towards observed climatological mean profiles of the open sea monitoring station P2 in the northern Kattegat (57°N 52′, 11°E 18′).*

each group are performed to make interpretation of results easier. In hindcast runs (H1 to H5) observed atmospheric forcing (or re-analysis data) and monthly mean, observed river runoff are used. The investigated period is May 1980 to December 1993.

In the hindcast runs the meteorological forcing is calculated from three hourly fields for sea level pressure, geostrophic wind components, air temperature in 2 m height, relative humidity in 2 m height, total cloud cover and precipitation from the Swedish Meteorological and Hydrological Institute (SMHI) database. To obtain the atmospheric

forcing, observations are interpolated on an one degree regular horizontal grid (Lars Meuller, pers. comm.). The wind is reduced to 10 m height according to Bumke et al. (1998). In experiment H2 these geostrophic based wind fields are replaced by 10 m winds of the ECMWF re-analysis (ERA, see Gibson et al. 1997). The other meteorological variables are taken from the SMHI database also in this run.

Two different RCO versions (RCO-a and RCO-b) are utilized to calculate model dependent uncertainties. In the version RCO-a surface fluxes are calculated from bulk formulae, as given in Appendices A and B. In the version RCO-b shortwave and incoming longwave radiation are modified according to Bodin (1979). In addition, some minor changes are performed (Tab.2).

subject	RCO-a	RCO-b
cloudiness function of incoming longwave radiation	$\propto (1 + 0.2232\, C_a^{2.75})$ (Maykut and Church 1973; see Appendix A)	$\propto (1 + 0.18\, C_a^2)$ (Bodin 1979; see Meier et al. 1999)
solar constant	$S_0 = 1.368 \cdot 10^3\, J\, m^{-2}\, s^{-1}$	$S_0 = 1.353 \cdot 10^3\, J\, m^{-2}\, s^{-1}$
cloud cover correction of solar radiation over ice	$\propto (1 - C_a^3\, F_a)$ (Laevastu 1960)	$\propto (1 - C_a\, F_a)$ (Bodin 1979)
albedos for dry and wet ice, dry and wet snow	0.7, 0.3, 0.87, 0.77 (Perovich 1996)	0.45, 0.2, 0.87, 0.77
min. permitted ice thickness	$h_{min} = 0.02\, cm$	$h_{min} = 0.04\, cm$
ice-ocean heat flux	$T_w - T_{fp} > 0^\circ C$	$T_w - T_{fp} > 0.1^\circ C$
snow ice model (flooding)	5 cm negative freeboard allowed (cf. Saloranta 2000)	no negative freeboard
$k - \epsilon$ model	reduced dissipation (see Meier 2000)	no reduction

Table 2: *Differences in the two RCO versions (RCO-a and RCO-b) used in the report. For details the reader is referred to Appendices A and B and to the description of RCO by Meier et al. (1999).*

In experiments H4 and S4 salinity is kept equal to zero to show the sensitivity of sea ice on surface salinity and to show the consequence of stratification for the scenario run. In experiment H5 Richardson number dependent friction has been used instead of the $k - \epsilon$ turbulence model resulting in underestimated mixed layer depths (Meier 2000). This experiment is performed to demonstrate the sensitivity of sea ice on the seasonal heat content in the ocean.

The river runoff data have been taken from the BALTEX (Baltic Sea Experiment) Hydrological Data Centre at SMHI. The monthly data do not only represent the inflow by major rivers, but the runoff through coastal segments including also estimated smaller runoff ways (Bergström and Carlsson 1994). In RCO the 29 most important coastal segments are considered.

As precipitation in the RCA control run is higher compared to present-day climate,

run C2 with increased river runoff from the control run is performed to show the sensitivity of stratification, during the time slice experiments, on the additional artificial fresh water input (10 year integration length). In the RCA control run, the 10-year mean runoff amounts to 19,958 m^3/s, whereas the 18-year mean for 1981-1998 is only 15,053 m^3/s (Tab.3). That is an increase of 32.6 %. The river discharges for this experiment and for both time slice experiments (control and scenario run) are calculated with a large-scale hydrological model (the HBV-Baltic model, Graham 1999), which is forced by daily mean air temperature and precipitation results from the RCA model simulations.

Observation	HBV hindcast	Control	Scenario	HBV hindcast plus change
15,310	15,053	19,958	21,154	16,311

Table 3: *Total river runoff into the Baltic Sea in m^3/s. The mean runoff from observations is calculated for the period 1950-1990 (Bergström and Carlsson 1994). The HBV-Baltic base condition is calculated for the 18-year period 1981-1998 (Graham 1999). The mean runoff for control and scenario run are 10-year means (Phil Graham 2000; pers.comm.). The last value denotes the 1981-1998 HBV-Baltic base condition with monthly temperature change and seasonal precipitation change from RCA1 (Phil Graham 2000; pers.comm.).*

In the control (C1, C3) and scenario experiments (S1 to S5) RCO is forced with data from RCA (Rummukainen et al. 2000; Räisänen et al. 2000), which is based on the High Resolution Limited Area Model, HIRLAM (Källén 1996). HIRLAM is used for numerical weather prediction in several European countries. Compared to HIRLAM, in RCA the land surface and snow schemes have been changed and separate modules have been added for inland lakes and the Baltic Sea. Here, data of the revised version of RCA (RCA1) are used with a rotated latitude-longitude grid of 88 km resolution and with 19 hybrid levels between the surface and 10 hPa. It is forced by the driving GCM from its lateral boundaries and from below, by Atlantic sea surface and deep soil temperatures. For the Baltic Sea surface RCA is fully coupled with the horizontally integrated model with 13 vertically resolved boxes by Omstedt (1990) and Omstedt and Nyberg (1996). Lake temperatures are also modeled in an interactive manner in the Baltic Sea drainage basin (the RCA model domain including the Baltic Sea and the area, where the lake module is applied, are shown in Fig.1 by Räisänen et al. 2000). The lake module (Ljungemyr et al. 1996) treats shallow (mean depth less than 10 m) lakes with a 0-dimensional energy balance model and deep lakes (mean depth over 10 m) with a vertically resolved model. Ice cover and ice thickness are also simulated in both the Baltic Sea and inland lake modules. A fully coupled RCA-RCO model is presently under development at the Rossby Centre.

The RCA simulations are dynamical downscaling experiments using boundary data from the global ocean-atmosphere circulation model from the Hadley Centre, HadCM2 (Johns et al. 1997; Mitchell and Johns 1997; cf. Räisänen and Döscher 1999). Two

10-year time slice simulations representing control (pre-industrial, approximately the fifties) and scenario (future) climate with 150% increased greenhouse gas concentrations compared to the control conditions are performed. No sulphate aerosol forcing is included in this GCM experiment. In the transient run gradually increasing CO_2 represents the change in greenhouse gas forcing from the pre-industrial era. The used period of the corresponding time slice experiments extends from 2039 till 2049. If one wants to interpret differences between the scenario and the control run as climate changes from the present to some period in the future, this future should be placed somewhere around the year 2100. The global mean temperature between the two time slices increases by $2.6°C$.

The climate in the RCA control run and its relation to the control climate in the driving GCM were discussed by Rummukainen et al. (2000). The GCM simulation was generally found to be of reasonably high quality for the Nordic region (compared with the errors typically present in current atmosphere-ocean GCMs), but some marked biases were also identified. HadCM2 was found to have a general cold bias in surface air temperature in spring and summer, which reaches $3-4°C$ in the Nordic Countries in July. Precipitation is above the CRU climatology (Hulme et al. 1995) in winter and spring and somewhat below it in summer. The biases in RCA followed more or less closely the driving GCM results. In Räisänen et al. (2000) the RCA scenario run is analyzed and discussed. The 10-year annual mean change (scenario minus control) in surface air temperature over the Baltic Sea area is between 2 and $3°C$ with somewhat larger increases in the Bothnian Bay and Gulf of Finland (see Fig.2 by Räisänen et al. 2000). In summer (June-August) the increase is smaller ($2-3°C$ over the entire Baltic) and in winter (December-February) higher ($3-4 °C$ over the Baltic proper and Bothnian Sea and $4-5°C$ over the Bothnian Bay and Gulf of Finland) than in the annual mean.

Using six hourly atmospheric data from RCA (sea level pressure, 10 m wind speed, 2 m air temperature, 2 m relative humidity, total cloudiness and precipitation), sea surface fluxes in RCO are calculated from the same bulk formulae as in the hindcast experiment (Appendices A and B). As the available record of forcing data starts in September, the heat content of initial temperature profiles would affect the first winter. Consequently, RCO has been started in May of the following year, before the spring thermocline starts to develop. Thus, the RCO integration length of control and scenario time slices is only 9.5 years.

5 Spin-up strategy

From the outlined experiment strategy a problem occurs in connection with the initial conditions for the scenario run. Here, it is assumed, that present-day temperature and salinity fields (from May 1980) could be used to initialize the future scenario time slice experiment as well. This assumption is questionable due to two reasons.

Firstly, precipitation and therefore river runoff are higher in the scenario run compared

with the control run. The change in runoff (scenario minus control run) calculated with the HBV-Baltic model is about 1,200 m^3/s (Tab.3). That is an increase of 6%. This additional amount of fresh water causes the Baltic Sea surface layer to drift to lower salinities.

Secondly, stratification in the Baltic Sea is very much dependent on salt water inflows, especially major salt water inflows (see Section 2). Due to these events the variability of bottom layer salinity in the Baltic proper has been quite high during the past 100 years (between 11 and 14 psu in 200 m depth at Gotland Deep). If changing climate will alter the frequency of salt water inflows, is an open question. If there is a lack in salt water inflows in future, the Baltic Sea deep layer will drift to lower salinities. The corresponding time scale of this drift is the longest in the estuarian system and is related to diffusion across the halocline. The typical residence time of the Baltic proper is about 30 years, much longer than the integration period of the time slice experiments.

Hence, a forecast, how haline stratification will develop within the next 100 years, is impossible without performing a reliable coupled atmosphere-ocean transient run. As outlined above, the observed decreased number of salt water inflows during the last 3 decades may be a hint, that salinity in the Baltic Sea could decrease in future. Although the forecast of salinity is impossible with the time slice approach, the uncertainty of predicted climate change for other variables like sea surface temperature or ice coverage can be estimated starting the scenario run from different realistic extremes, representing future variability. As future variability may be very different from present-day variability, these extremes cannot be taken from extreme observations of the past 100 years (since observations exist). First of all, the worst case has been assumed with no information about salinity at all. Hence, in an additional scenario run the Baltic Sea has been treated as a lake without haline stratification (salinity equal to zero, S4, see Tab.1). The results have been compared with the standard scenario run (S1) initialized with present-day haline conditions (see next section). As, for example, details of the results for seasonal mean sea surface temperature change show quite large differences (defined as uncertainties of the predicted climate change signal), the spin-up strategy in this report is refined. RCO is used in a sub-cycling experiment to spin-up initial conditions for the scenario time slice run in 90 years, using the same 9-year forcing fields from the RCA scenario run repeatedly 10 times (S2). Thereby, again the worst case has been assumed, so that the result could be regarded as extreme future projection with lowest possible haline stratification. Sea level elevations in Kattegat during each sub-cycle are prescribed from observations for the period May 1980 until April 1989. Consequently, no major salt water inflow occurred (as in hindcast and control experiments). River runoff in the spin-up experiment is calculated with the HBV-Baltic model from observations plus the relative change of scenario minus control run. In the calculations the monthly temperature change and the seasonal precipitation change (winter, spring, summer, fall) from RCA are used (Phil Graham 2000; pers.comm.). The increase compared to the hindcast run is 8% (Tab.3). In the next section results of both scenario experiments without and with spin-up (S1 and S2) are compared with the control run (C1).

6 Results

In this section, results of hindcast, control and scenario runs are presented. Thereby, the focus is on time evolution of salinity in the Baltic proper, annual and seasonal mean sea surface temperature (SST), ice extent variability, mean maximum annual ice thickness, mean ice season length, mean sea surface height (SSH) and mean maximum annual SSH.

6.1 Vertical profiles of salinity

In Fig.2, observed and simulated isohaline depths at Gotland Deep (BY15) in the eastern Gotland Basin are shown. The observations include 153 profiles between May 1980 and December 1993. During the stagnation period salinity in the deeper layer of the Baltic Sea decreased remarkably (between May 1980 and December 1992 by about 2 psu), because almost no saltier water originating from the North Sea was advected horizontally into the Gotland Deep. The results of the hindcast experiment (H1, Fig.2b) are in good agreement with the observations. As shown by Meier (2000, Fig.16c), there is no systematic bias in the deep layer salinity in RCO and only a small bias (i.e., higher model salinities) in the upper layer of 0.1 to 0.4 psu after 13.6 years of simulation. However, the gradient of the upper halocline is slightly reduced by the model. The control run (C1, Fig.2c) shows very similar salinity evolution than in the hindcast run, but the halocline is sharper, bottom salinity after 9.5 years is slightly higher (0.1 to 0.4 psu), and surface layer salinity is lower (-0.5 to -0.8 psu; Fig.3a). The halocline in the scenario run (S1, Fig.2d) is somewhat deeper than in the control run and surface layer salinity is lower with -0.2 to -0.5 psu (Fig.3b).

To explain the differences, two sensitivity experiments for the hindcast period have been performed with increased runoff calculated with the HBV-Baltic model from the control run (C2) and with ERA wind forcing instead of the geostrophic based winds from the SMHI database (H2). The corresponding differences with the standard hindcast run are shown in Fig.3c and Fig.3d, respectively. The additional river runoff of the control run of about 4,900 m^3/s reduces surface layer salinity by -0.5 to -0.8 psu after 10 years and causes a deeper halocline. Thus, the reduced surface layer salinity of the control run, compared with the hindcast run, can be explained partly by additional freshwater forcing (including a smaller contribution from net precipitation). In the scenario run the even higher runoff (1,200 m^3/s more than in the control run, see Tab.3) reduces surface layer salinity further and deepens the halocline compared to the control run. It is important to note, that additional river runoff does not influence bottom salinity. The differences of halocline gradients and salinities in the deeper layer are caused by differences between different wind forcings. In coarse resolution atmosphere models (e.g. ERA, RCA) simulated 10 m wind speeds with amplitudes higher than 10 m/s are typically underestimated systematicly compared to observations, whereas geostrophic based wind speeds used in the standard hindcast run with amplitudes higher than 10 m/s are overestimated. Higher wind speeds cause increased diapycnical mixing in the deep layer and across the halocline (Ekman pumping/suction). Thus, bottom salinity is slightly higher and halocline gradients are sharper in the control run (C1) compared
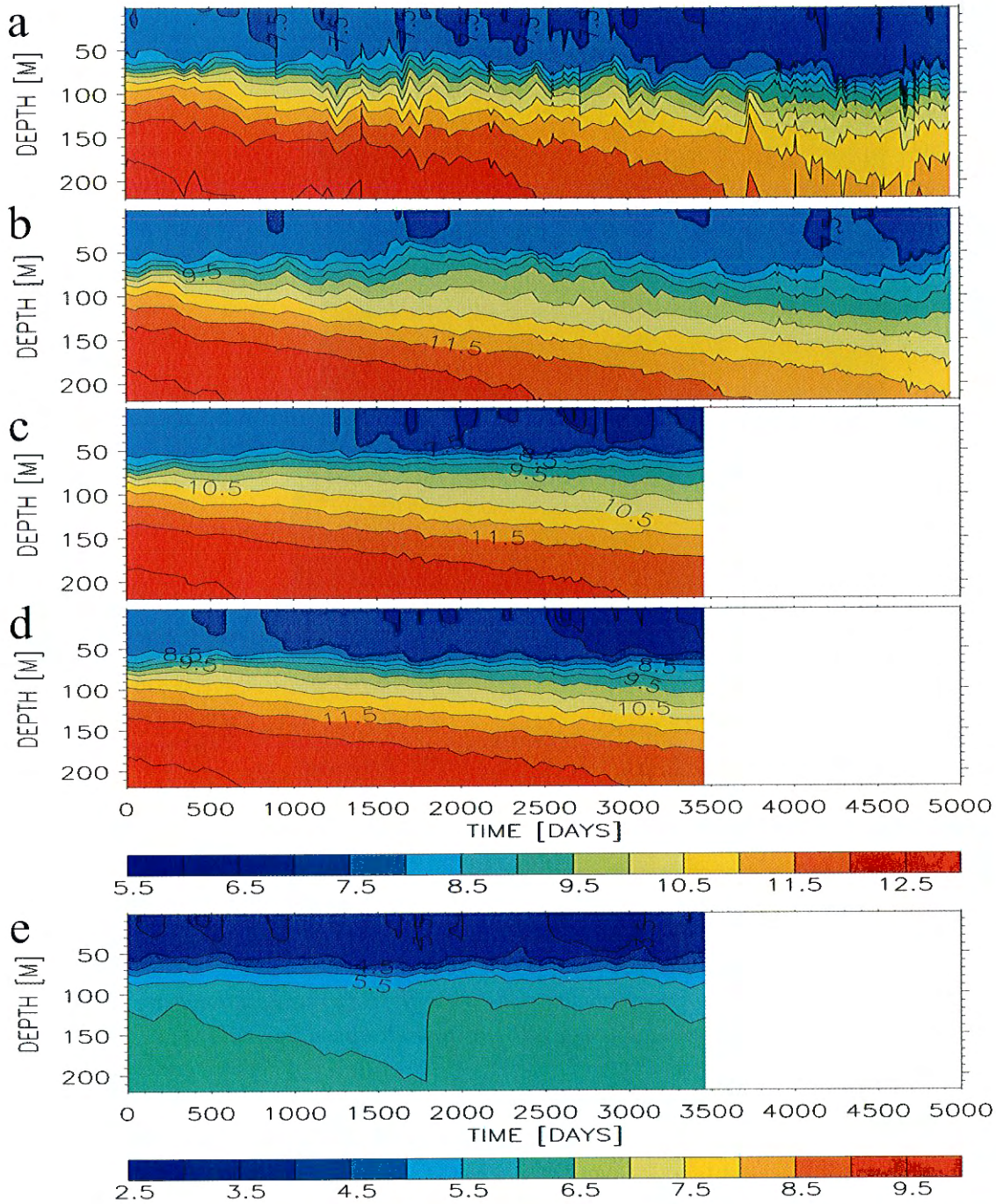
Figure 2: *Observed (a) and simulated (b-e) isohaline depths (in psu) at Gotland Deep (BY15): (b) hindcast run (H1), (c) control run (C1), (d) scenario run (S1) and (e) scenario run after 90 years of spin-up time (S2). Note the different color bar in (e).*

to the hindcast run (H1), (Fig.3a), and in the hindcast run with ERA wind forcing (H2) compared to the hindcast run (H1), (Fig.3d).

During the 99.5-year integration of the scenario run S2, salinity in the Baltic Sea decreases tremendously due to diffusion across the halocline and due to increased river
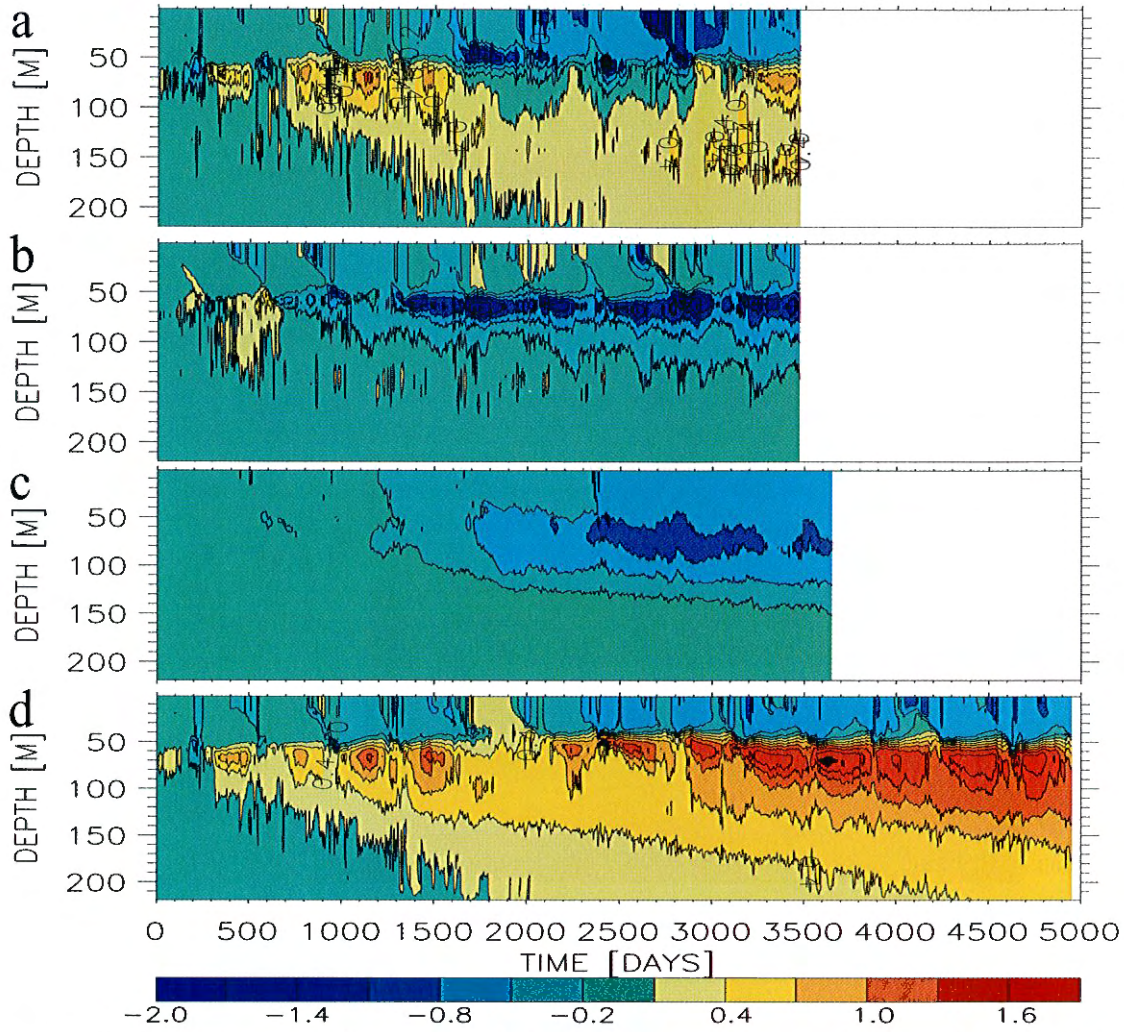
Figure 3: *Differences of simulated isohaline depths (in psu) at Gotland Deep (BY15): (a) control run (C1) minus hindcast run (H1), (b) scenario run (S1) minus control run (C1), (c) control run with only increased river runoff (C2) minus hindcast run (H1), (d) hindcast run with ERA wind forcing (H2) minus standard run (H1).*

runoff (Fig.4b). The comparison of the last 9.5 years of the scenario run S2 (Fig.2e) with the control run C1 (Fig.2c) shows that salinity in the deep layer has decreased by about 6 to 6.5 psu and in the surface layer by about 3 to 4 psu. However, there is still a remarkable stratification present with a halocline between 50 and 150 m depth. Sea surface and bottom salinity are 3-4 and 6-6.5 psu, respectively. Salinity does not decrease further, because an inflow event every 9 years (after about 1800 days of each sub-cycle) renews the deep water continuously. During the first decades overflowing water from the sill between Bornholm and Gotland Basin (Stolpe Channel) replaces water in the upper halocline evident from the temperature record (Fig.4a). After salinity in the bottom layer has decreased correspondingly, the overflow water replaces also bottom water. Now, bottom salinity in the Baltic proper increases by about 0.4 psu during each salt water inflow, compensating the salinity loss due to diffusion in 9 years. After 100 years the system is in quasi-equilibrium approximately.

14
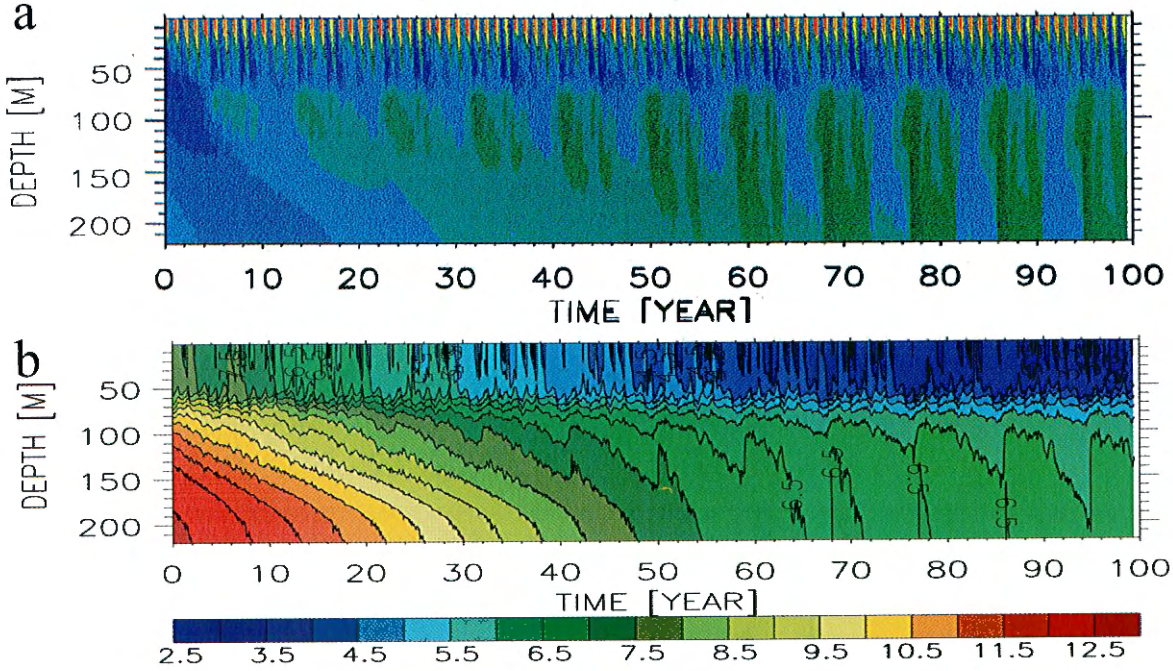
Figure 4: *(a) Isotherm depths (in °C) and (b) isohaline depths (in psu) at Gotland Deep (BY15) during the 99.5-year spin-up (S2).*

6.2   Sea surface temperature

Temperature and salinity in the standard hindcast simulation (H1) are found to agree well with observations. A comparison of observed and simulated median, first and third quartile profiles from different basins has been presented by Meier (2000). The model reproduces salinity gradients from North to South as well as from the surface to the bottom quite well. Also median temperature profiles and its variability are in agreement with observations. A revised heat flux package and an improved $k - \epsilon$ turbulence model contribute to the good results.

Here, the focus is on SSTs. Model results of four different basins are shown in Fig.5 and compared with available data from corresponding monitoring stations. Mean errors are $\pm 0.1°C$ except for the Bornholm Basin ($0.4°C$, Tab.4). Root mean square errors are only slightly higher than $1°C$ in all basins (highest in the Gulf of Finland with $1.3°C$, Tab.4).

In Fig.6, monthly mean sea surface temperature differences are shown. In the northern sub-basins only during the summer months May to November a sufficient number of observations is available. SST biases in RCO are smaller than natural variability and are of the order $\pm 1°C$. The larger seasonal cycle in RCO is explained by the fact that mainly land stations are included in the SMHI database.

15
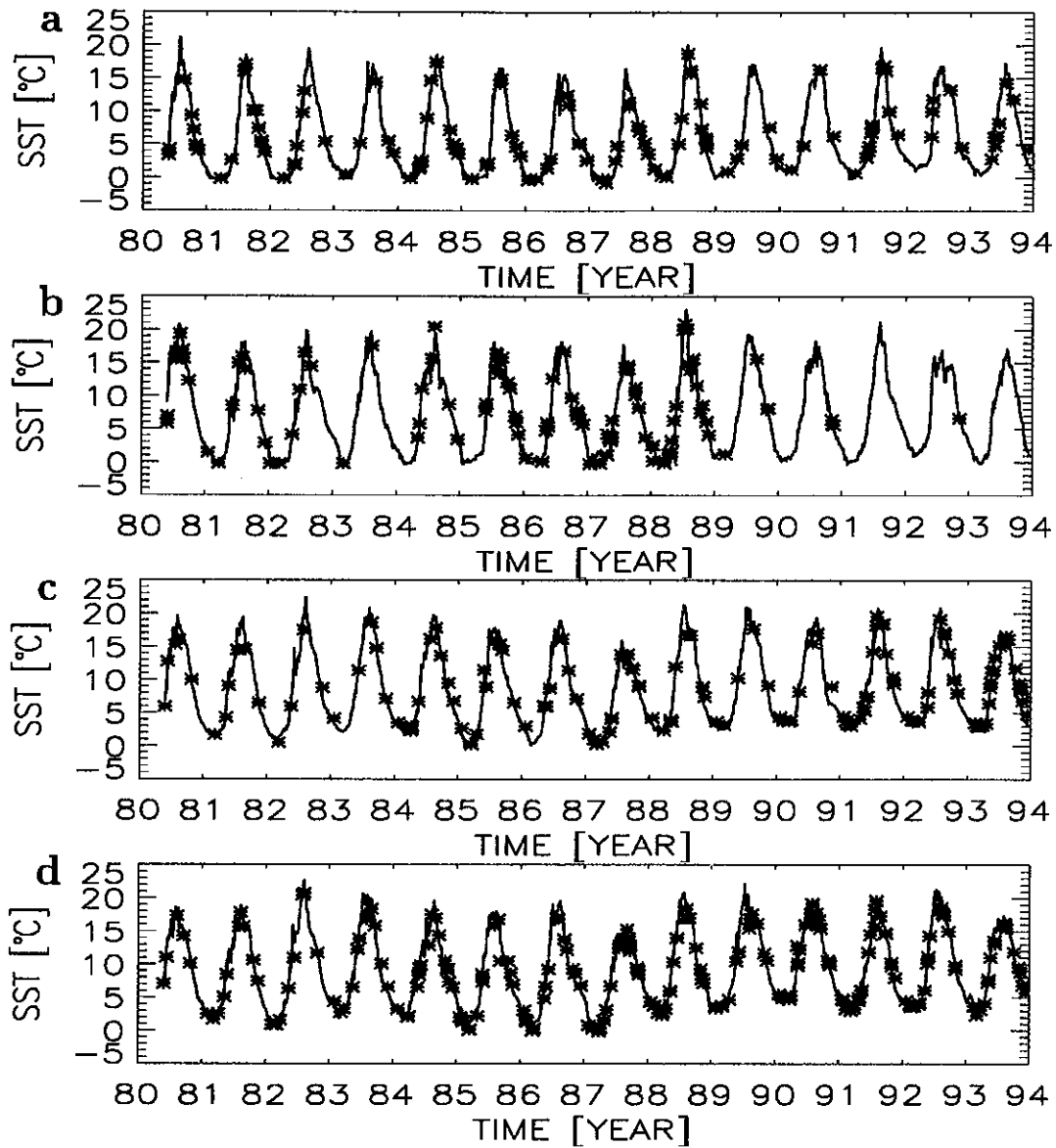
Figure 5: *Simulated (solid, run H1) and observed (asterisk signs) sea surface temperature (in °C) from the period May 1980 until December 1993 at SR5 in the Bothnian Sea (a), LL07 in the Gulf of Finland (b), BY15 in Gotland Basin (c) and BY5 in Bornholm Basin (d). Positions are shown in Figure 1.*

In Fig.7, annual and seasonal mean SSTs of the control run (C1) are shown and compared with the hindcast run (H1). The bias of the annual mean SST is smaller than 1°C with a positive bias in the Bothnian Sea and Bothnian Bay and a negative bias in the central and northern Gotland Basin and in the south-western Baltic. In autumn and winter SSTs in almost the entire model domain are warmer in the control run. The largest positive differences between control and hindcast results occur in winter in the southern Gotland Basin and in autumn in the central Bothnian Sea ($> 1.8\,°C$). In spring SSTs in the southern and central Baltic Sea and in summer in almost the entire

16

Station	Position	Number	ME	RMSE
SR5	61°N 05.0′, 19°E 35.0′	124	0.1	1.1
LL07	59°N 50.5′, 24°E 50.3′	103	-0.1	1.3
BY15	57°N 20.0′, 20°E 03.0′	151	0.1	1.2
BY5	55°N 15.0′, 15°E 59.0′	244	0.4	1.0

Table 4: *Mean error (ME) and root mean square error (RMSE) of sea surface temperature (in °C) from the period May 1980 until December 1993 at monitoring stations SR5 in the Bothnian Sea, LL07 in the Gulf of Finland, BY15 in Gotland Basin and BY5 in Bornholm Basin. Positions are shown in Fig.1. The data are depicted in Fig.5. In addition, numbers of observations are listed.*
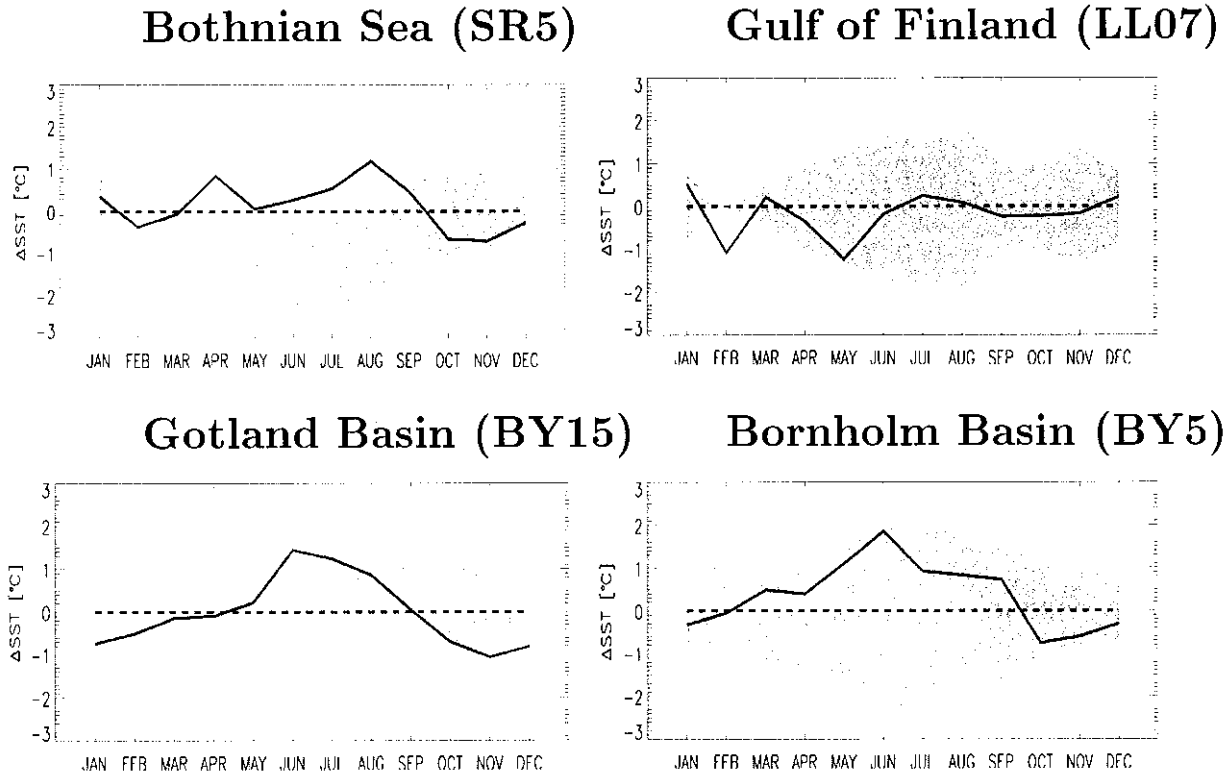
Figure 6: *Monthly mean sea surface temperature differences between model results (H1) and observations. The same sub-set of stations as in Fig.5 is shown. The shaded areas indicate observed natural variability defined by the standard deviation. By definition, standard deviation is set to zero, if only one of the possible 13 values per month includes data (the case, that a month contains no data, does not occur).*

Baltic Sea are colder in the control than in the hindcast run. The largest negative differences are found in the central Gotland Basin around Gotland ($< -2.6\,°C$). The spring/summer cold bias in SSTs follows a corresponding 2 m air temperature bias in

ANNUAL   DJF   MAM   JJA   SON
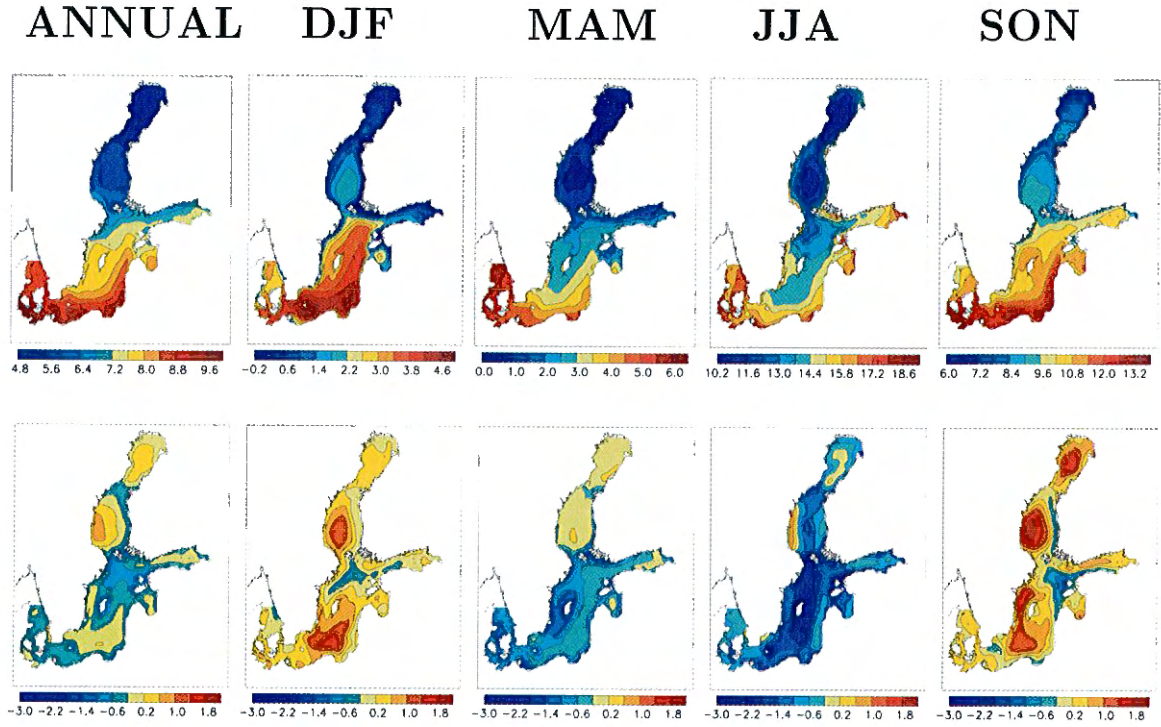
Figure 7: *Upper panel: Sea surface temperature (in °C) of the control run (C1). From left to right, the 9-year annual mean and seasonal means for winter (December-February=DJF), spring (March-May=MAM), summer (June-August=JJA) and autumn (September-November=SON) are depicted. Note the different color bars. Lower panel: As the upper panel but corresponding differences between control (C1) and hindcast run (H1).*

HadCM2 and consequently RCA (Räisänen and Döscher 1999; Rummukainen et al. 2000). However, the autumn/winter warm bias is caused by an increase of incoming longwave radiation due to higher total cloudiness in the RCA control run compared to the SMHI database.

The annual and seasonal mean SST changes (scenario minus control run) are shown in Fig.8 and Fig.9, respectively. In addition, two changes are compared to each other: the difference between standard scenario (S1) and control run (C1) and the difference between scenario run with spin-up (S2) and control run (C1). In Tab.5 the corresponding area mean SST changes for the Baltic Sea (excluding the Kattegat) are listed. The annual mean SST change is about 2.3°C, averaged over the Baltic Sea without Kattegat, in both scenario experiments. Maxima ($> 2.6\,°C$) are found in the eastern Bothnian Sea, southern Gulf of Finland, central Gotland Basin and Bornholm Basin. Near the Swedish coasts, in the northern Bothnian Bay and at the east end of the Gulf of Finland the warming is only about $2\,°C$ or locally even smaller. Minimum change occurs in the Kattegat close to the open boundary, because in case of inflow temperature profiles are nudged towards present-day climatology in control and scenario simulations. The differences between the two scenario experiments are small in the annual mean and do
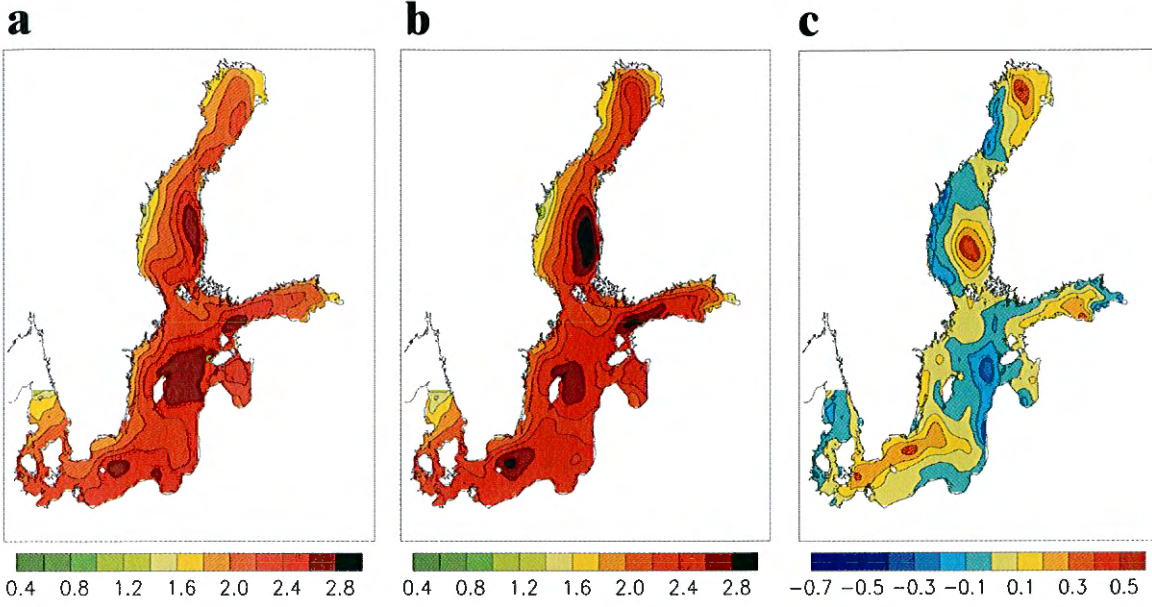
Figure 8: *Change of annual mean sea surface temperature (in °C). (a) scenario (S1) minus control run (C1), (b) scenario run after 90 years of spin-up time (S2) minus control run (C1), (c) difference between (b) and (a). Note the different color bar in (c).*

	Experiment	Annual	DJF	MAM	JJA	SON
a	S1 - C1	2.28	2.24	2.65	2.50	2.02
b	S2 - C1	2.33	2.54	2.70	2.03	2.03
c	S2 - S1	0.04	0.30	0.06	-0.48	0.01
d	S3 - C3	2.43	2.18	2.68	2.61	2.25
e	(S3 - C3) -(S1 - C1)	0.15	-0.06	0.04	0.10	0.23
f	S4 - C1	2.34	2.83	2.78	1.82	1.95
g	S4 - S1	0.06	0.59	0.13	-0.69	-0.07

Table 5: *Changes of area mean sea surface temperatures (in °C) excluding Kattegat for the standard scenario experiment without (a) and with spun up initial conditions (b). (c) shows the differences between these two changes. In (d) the modified version RCO-b has been used and in (e) the differences between (d) and (a) are listed. In (f) the scenario run with zero salinity is utilized and in (g) the differences between (f) and (a) are tabulated.*

not exceed the range between -0.4 and 0.5 °C locally (Fig.8c).

The largest warming of more than 3.8°C is simulated in the Bay of Bothnia and Bothnian Sea in summer using the standard scenario experiment (Fig.9). Contrary, warming of SST is smallest in the northern parts of the Baltic in winter and spring, because these areas are still ice covered in the scenario run. As ice extent is smaller in the
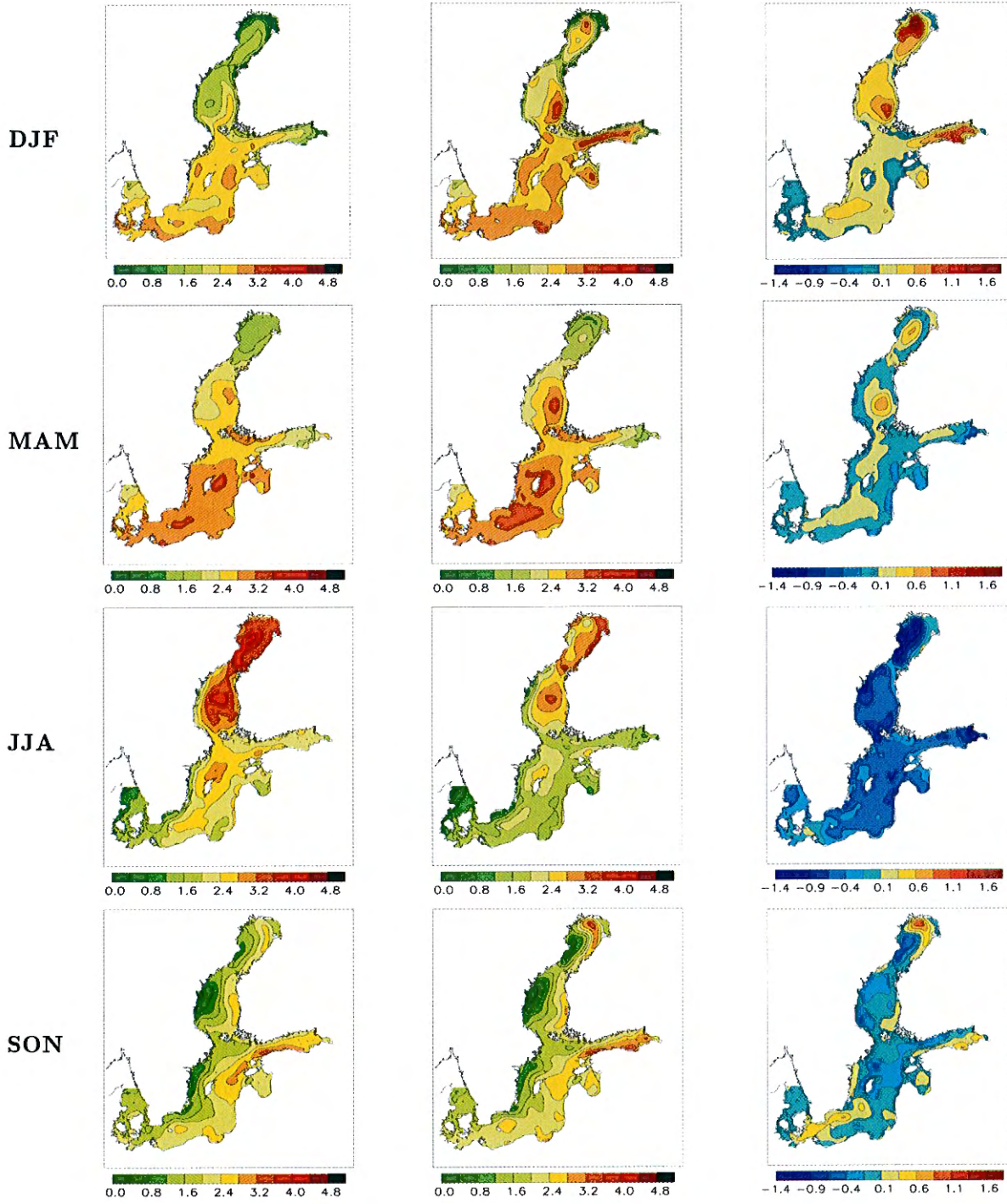
Figure 9: *Changes of seasonal mean sea surface temperatures (in °C). Left column: scenario (S1) minus control run (C1), center column: scenario run after 90 years of spin-up time (S2) minus control run (C1), right column: difference between second and first column. From top to bottom winter (DJF), spring (MAM), summer (JJA) and autumn (SON) are depicted. Note the different color bar in case of the difference.*

20

a   **b**   **c**

0.4   0.9   1.4   1.9   2.4   2.9   3.4   0.4   0.9   1.4   1.9   2.4   2.9   3.4   −0.7   −0.3   0.1   0.5   0.9
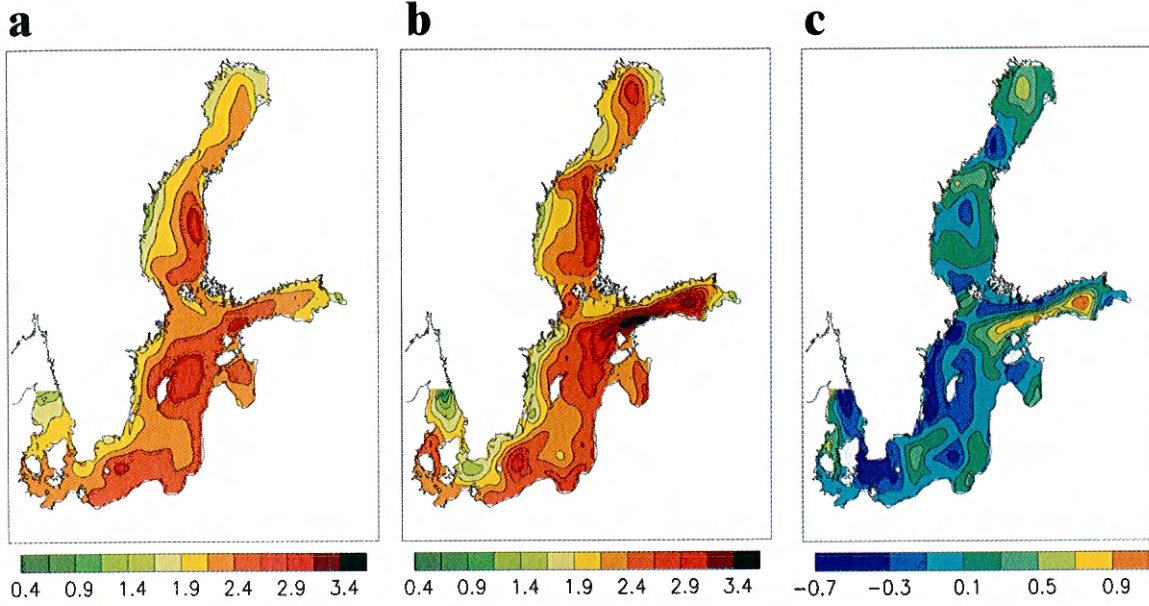
Figure 10: *Change of annual mean sea surface temperature (in °C): (a) scenario (S1) minus control run (C1), (b) scenario run with zero salinity (S4) minus control run (C1), (c) difference between (b) and (a). Note the different color bar in (c).*

scenario simulation (see next subsection), only those regions will warm up, where the ice has vanished in the mean, i.e., in the Bothnian Sea in spring. In autumn a pronounced east-west asymmetry in the entire model domain is found. Upwelling areas are warmed by less than $1.2\,°C$, whereas downwelling areas are warmed by more than $2.4\,°C$ or even higher (in the South of the Gulf of Finland). This signal is so intense, that also the annual mean is affected (Fig.8a,b).

Seasonal area mean changes in the scenario run with spin-up do not differ by more than $\pm0.5\,°C$ with the largest deviation in summer (Tab.5). Also similar horizontal anomaly patterns are found in this scenario, but there are local differences as well (Fig.9, center column). The right column in Fig.9 shows the differences, i.e., a measure of the uncertainty due to the unknown initial conditions. In general, these differences are in the range between - 1.4 and $1.8\,°C$, i.e., smaller than the simulated climate change signals. The largest positive and negative differences are found in winter and summer, respectively, both in the Bothnian Bay. Consequently, the simulated climate change in the northernmost basin with the weakest haline stratification is the most uncertain. Although present-day stratification is small, it limits mixed layer depths effectively. With even smaller stratification in the scenario experiment S2 summer mixed layer depths increase and SSTs decrease consequently.

Contrary, if it is assumed that the Baltic Sea will be a lake in future (with zero salinity), corresponding SST differences will be much larger locally (Fig.10 and Fig.11). Even in the annual mean, differences between the changes (S4 minus S1) of more than $0.9°C$ occur in the Gulf of Finland. This signal is very intense in winter (Fig.11). In summer SST warming in S4 is smallest, because a deeper seasonal thermocline compensates the additional heat input into the ocean. The differences between area mean changes

21
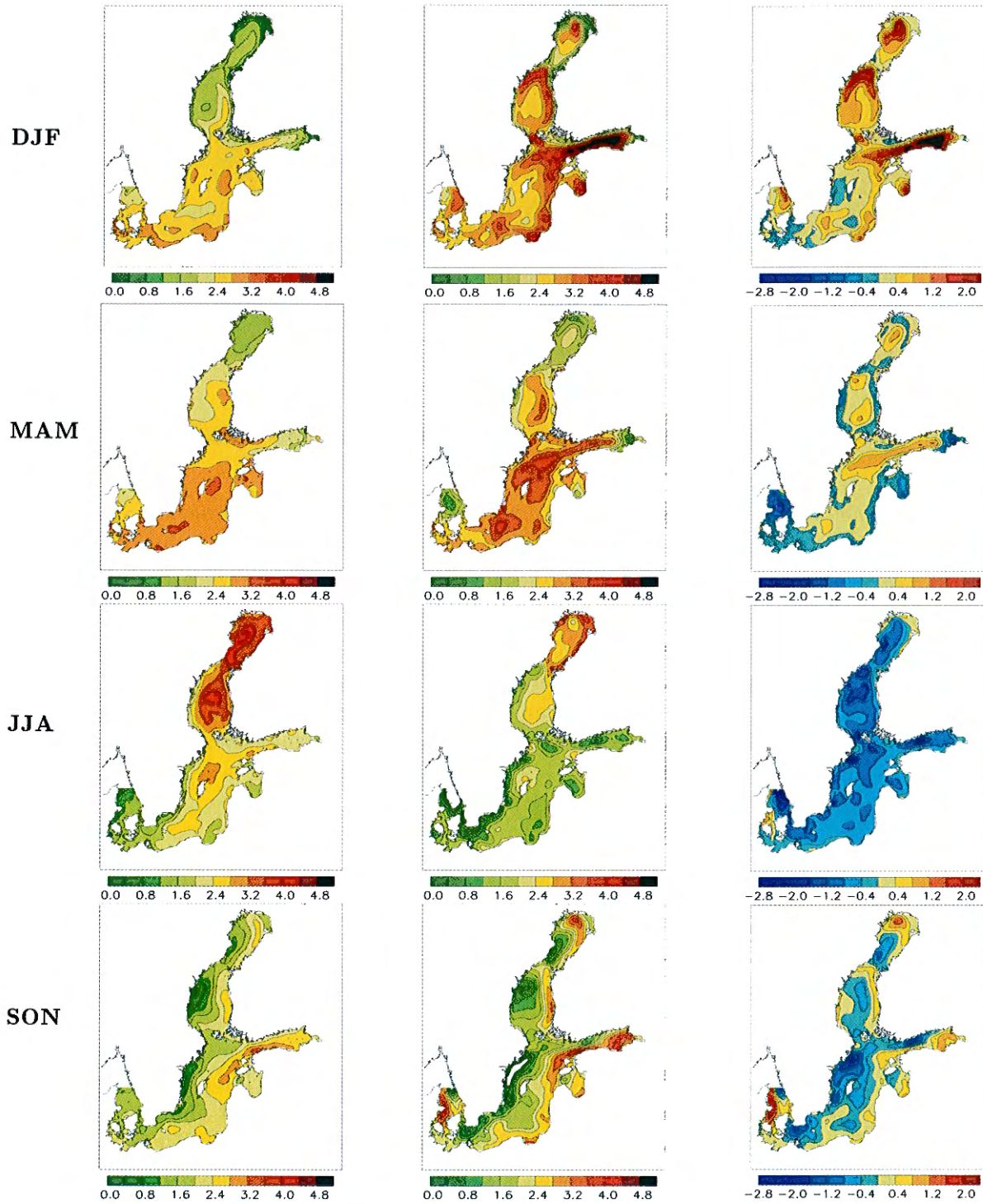
Figure 11: *Changes of seasonal mean sea surface temperatures (in °C). Left column: scenario (S1) minus control run (C1), center column: scenario run with zero salinity (S4) minus control run (C1), right column: difference between second and first column. From top to bottom winter (DJF), spring (MAM), summer (JJA) and autumn (SON) are depicted. Note the different color bar in case of the difference.*

amount to $0.59°C$ in winter and to $-0.69°C$ in summer (Tab.5).

In addition, the comparison with area mean 2 m air temperature is interesting. Corresponding changes of annual, winter, spring, summer and autumn means are $2.9°C$, $3.5°C$, $2.9°C$, $2.4°C$ and $2.6°C$, respectively (Jouni Räisänen 2000; pers.comm.). Obviously, the higher temperature change in the atmosphere in winter does not warm the water body to the same amount, because still available sea ice in the scenario run isolates it.

6.3 Sea ice

6.3.1 Hindcast simulations

Prognostic variables of the ice model are ice velocities, ice thickness, ice concentration, snow thickness, heat content of brine, surface temperature, snow (one layer) and ice temperatures (two layers). As long-term observations for most of these variables are largely missing, the validation is focused on ice extent, monitoring data of ice and snow thickness and ice concentration from satellite data in the Bay of Bothnia. Horizontally resolved statistical data processed from ice charts are available, too (SMHI and FIMR 1982). However, these observations cover the period 1963-1979 with, on average, more severe winters than during the simulation period 1980-1993 making a direct comparison of results difficult.

Fig.12a shows simulated total ice extent compared with the observed maximum ice extent. Ice extent is highly correlated with air temperature, but it represents also a sensitive measure of ice model performance (albedos, ice-ocean heat flux, etc.). The mean simulated (observed) maximum ice extent is $196 \cdot 10^9 \, m^2$ ($181 \cdot 10^9 \, m^2$), the minimum is $91 \cdot 10^9 \, m^2$ ($52 \cdot 10^9 \, m^2$), and the maximum is $356 \cdot 10^9 \, m^2$ ($405 \cdot 10^9 \, m^2$). The correspondence between model results and observations in Fig.12a is encouraging. In some mild winters maximum ice extent is somewhat overestimated. However, the overall agreement is good (Tab.6). The mean error is $15 \cdot 10^9 \, m^2$ (model overestimation of about 8 %) and the root mean square error is $39 \cdot 10^9 \, m^2$. The model simulation shows also high skill for the date, when the maximum ice extent occurred. In Tab.6 two alternatives of observed date of maximum ice extent are listed. The first one is based upon data from the Finnish Institute of Marine Research (FIMR) and the second one from the SMHI. There is only one exception (winter 1988/89), when the ice model predicted a higher ice extent much earlier than the observations. However, there is also a disagreement between the two data sets of 39 days. Without this runaway winter, the mean error is -2 days and the root mean square error is 11 days for the SMHI ice data. The skill is even higher if the model results are compared with FIMR ice data.

In Figures 12b and 12c, simulated ice and snow thickness are compared to measurements at the coastal station Kemi in the northern Bothnian Bay. The data are published in reports of the FIMR (Finnish Marine Research 1982, Kalliosaari and Seinä
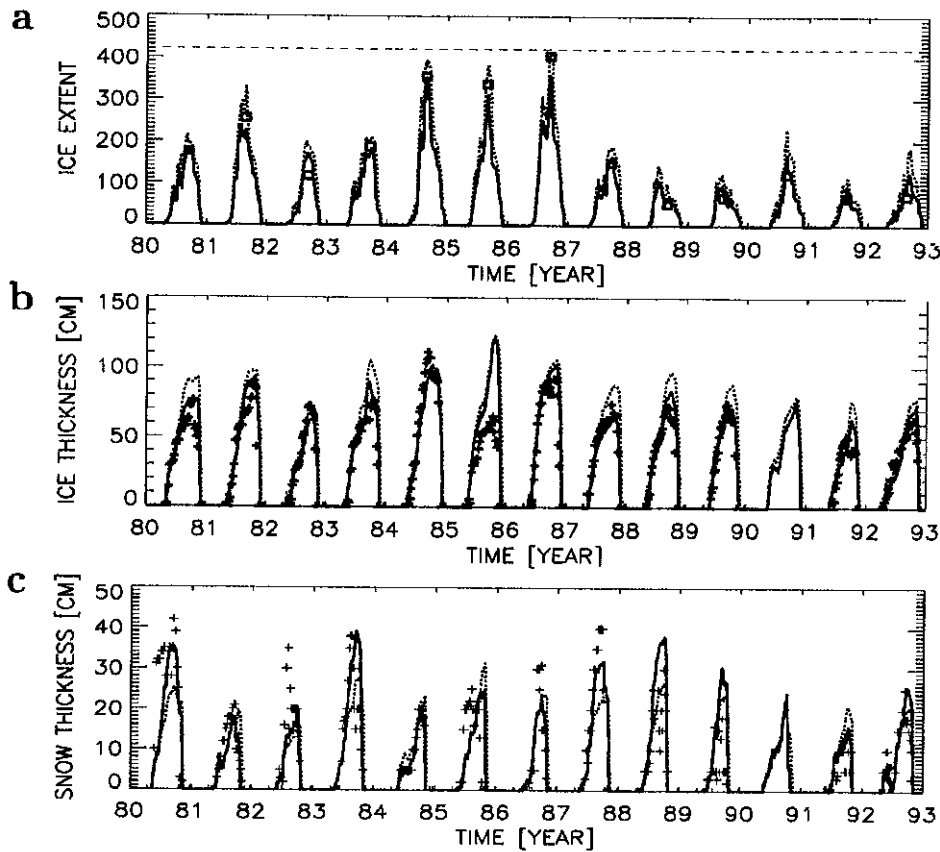
Figure 12: *(a) Simulated ice covered area (in $10^9\,m^2$) for the period July 1 1980 until June 30 1993. Squares denote observed maximum ice extent (cf. Omstedt and Nyberg, 1996). (b) Simulated ice and (c) snow thickness (in cm) at the monitoring station Kemi in the Bothnian Bay (see Fig.1). Plus signs denote observations from Finnish Marine Research (1982), Kalliosaari and Seinä (1987), Seinä and Kalliosaari (1991), Seinä and Peltola (1991) and Seinä et al. (1996). The winter 1990/91 data are not available. Tickmarks denote July 1. Solid lines show the standard run (H1) and dotted the sensitivity run with icier climate (H3). The dashed line in (a) denotes the Baltic Sea surface area including Belt Sea, Sound and Kattegat (420,560 km^2).*

1987, Seinä and Kalliosaari 1991, Seinä and Peltola 1991, Seinä et al. 1996). Inter-annual variability of maximum ice thickness in the Bothnian Bay is smaller than in case of ice cover. The agreement between model results and observations is regarded as very good, although the ice thickness during the severe winter 1985/86 is overestimated and although snow thickness is underestimated during some years (e.g., 1982/83). However, one has to keep in mind, that the precipitation data from the SMHI database might have a large error (the monitoring stations are located at land including some islands) and that the used snow ice model is quite simple. Precipitation over sea ice is assumed to be converted to snow and snow is converted to snow ice, if flooding occurs. As negative freeboard conditions in the Baltic fast ice area last up to months (Saloranta 2000), a negative freeboard of up to 5 cm is allowed. Ice and snow thicknesses are very

24

year	max ice extent ($10^9\,m^2$)			date (model errors in days)				
	data	model	Δ	data FIMR	data SMHI	model	Δ_{FIMR}	Δ_{SMHI}
1981	175	180	5	0317	0316	0317	0	1
1982	255	237	-18	0223	0226	0125	-29	-32
1983	117	170	53	0303	0312	0303	0	-9
1984	187	182	-5	0323	0322	0326	3	4
1985	355	354	-1	0222	0221	0225	3	4
1986	337	314	-23	0302	0227	0303	1	4
1987	405	356	-49	0316	0313	0314	-2	1
1988	149	163	14	0319	0319	0323	4	4
1989	52	109	57	0119	0227	1228	-22	-61
1990	67	95	28	0118	0131	0121	3	-10
1991	122	171	49	0220	0219	0220	0	1
1992	66	91	25	0221	0220	0223	2	3
1993	70	125	55	0225	0224	0305	8	9
ME			15				-2 (-1)	-6 (-2)
RMSE			35				11 (9)	20 (11)

Table 6: *Observed and simulated maximum ice extent (Δ = model error, ME = mean error, RMSE = root mean square error). The data are adopted from Omstedt and Nyberg (1996). The mean error and the root mean square error of the date of maximum ice extent without the runaway winter 1989 are given in brackets.*

sensitive on changes within the snow ice model.

In Fig.12, the additional dotted line denotes results calculated with RCO-b (H3). This hindcast simulation shows good performance compared to observations as well, but ice extent and ice thickness are slightly overestimated. As the slightly better performance of RCO-a might be caused only by compensating errors in the surface heat flux package (i.e. radiative fluxes) and in the meteorological forcing data (see discussion), both versions are used in scenario simulations to illustrate the uncertainty of results on utilized heat flux parameterizations (including the heat flux between ice and ocean). In the following, both ensembles (scenarios with RCO-a and RCO-b) are assumed to be equally realistic.

Information of horizontal distribution of ice thickness and ice concentration is included in ice charts drawn from observations and published by SMHI regularly twice a week. Three examples from a normal (1983/84), severe (1986/87) and mild (1991/92) ice winter, close to the date of maximum ice extent, are shown in Fig.13, Fig.14 and Fig.15, respectively. Although in RCO only one ice class is considered, the simulated ice thickness field shows similarity with the observations. In Fig.13, simulated maxima in the northern Bothnian Bay fast ice zone ($>75\,cm$) and in the central Bothnian Bay ($>60\,cm$) and the minimum of very thin or new ice in the central Bothnian Sea ($<5\,cm$) occur in the observations as well. During the severe winter 1986/87 almost the entire Baltic is frozen (Fig.14). Only in the southern Baltic proper open water is observed. Simulated ice thickness in the Bothnian Bay is somewhat too thick (Fig.14, upper panel). During the mild winter 1991/92 simulated ice extent is slightly overes-
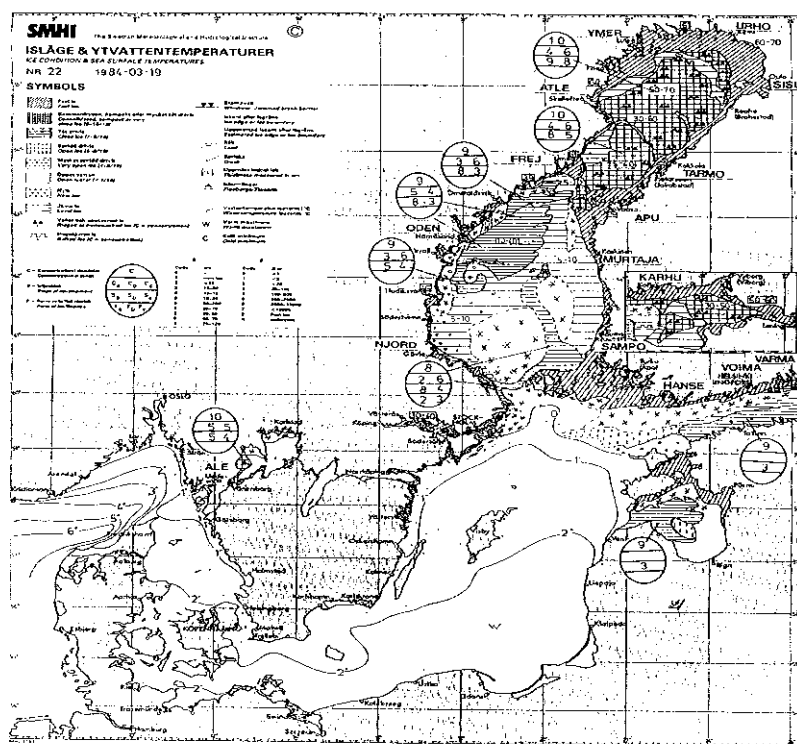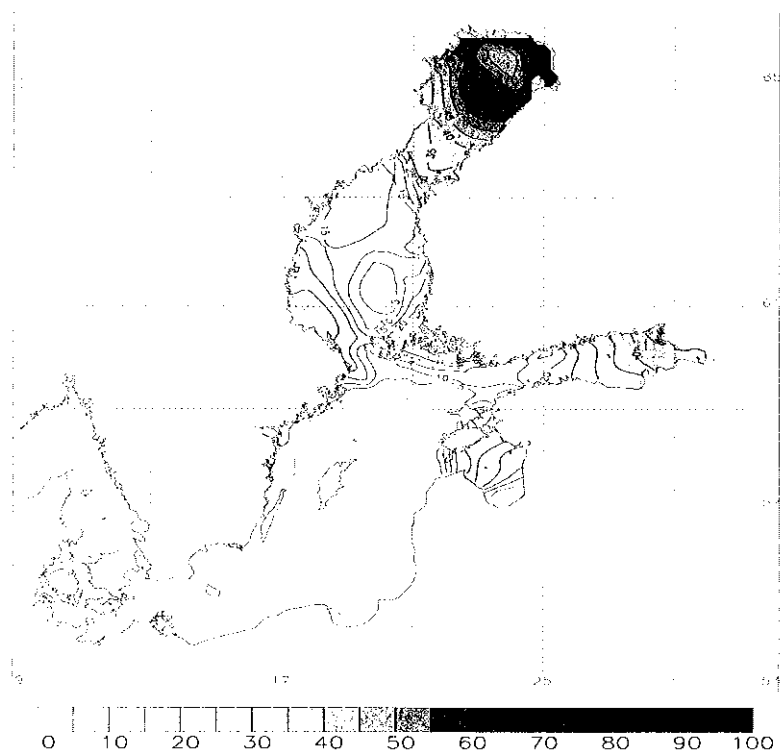
Figure 13: *Simulated ice thickness (in cm) on March 23 1984 (H1, upper panel), compared with the corresponding ice chart (lower) published by SMHI. The magnified key of the lower panel is shown in Fig.27.*
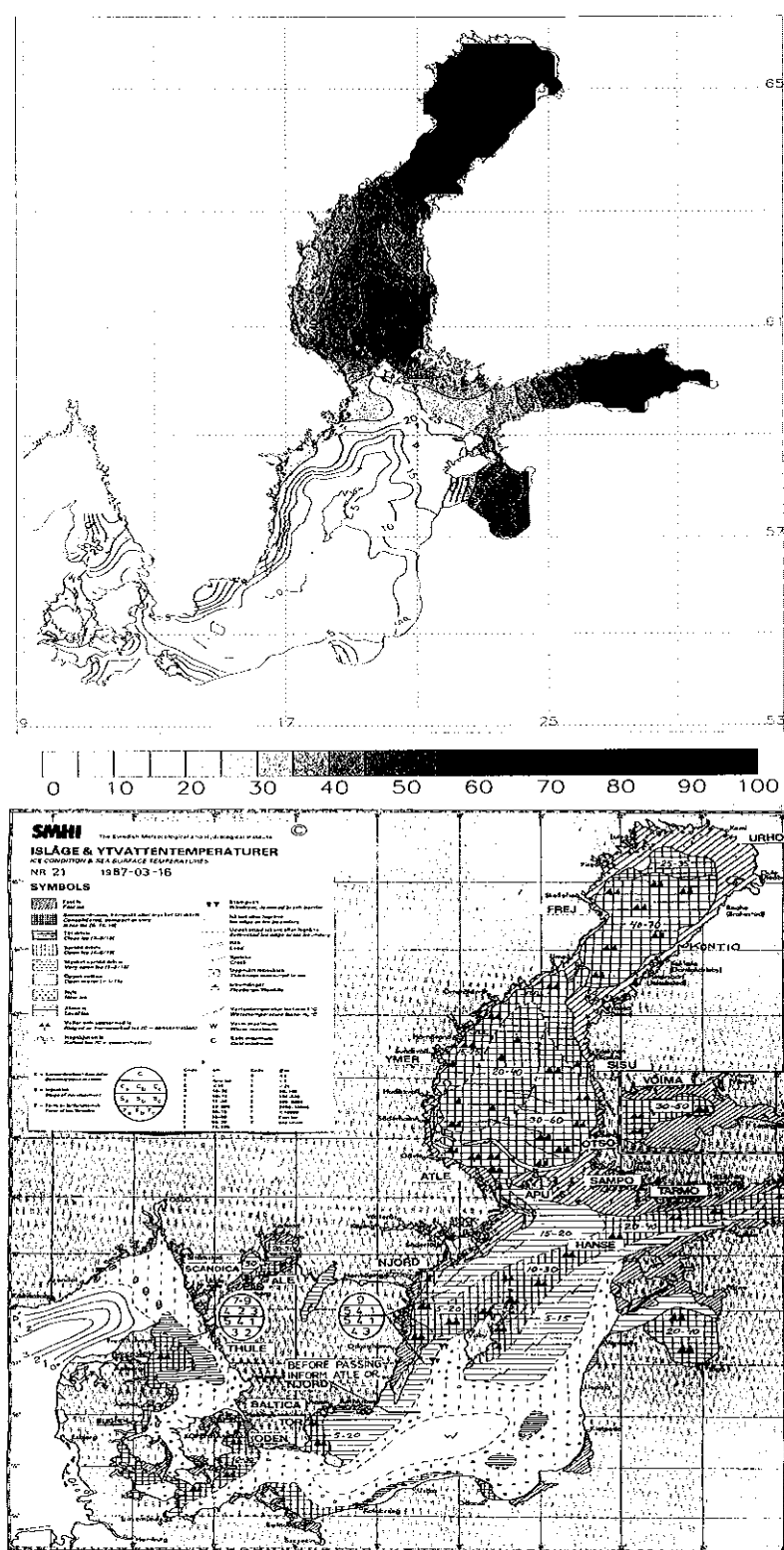
Figure 14: *Simulated ice thickness (in cm) on March 14 1987 (H1, upper panel), compared with the corresponding ice chart (lower) published by SMHI.*
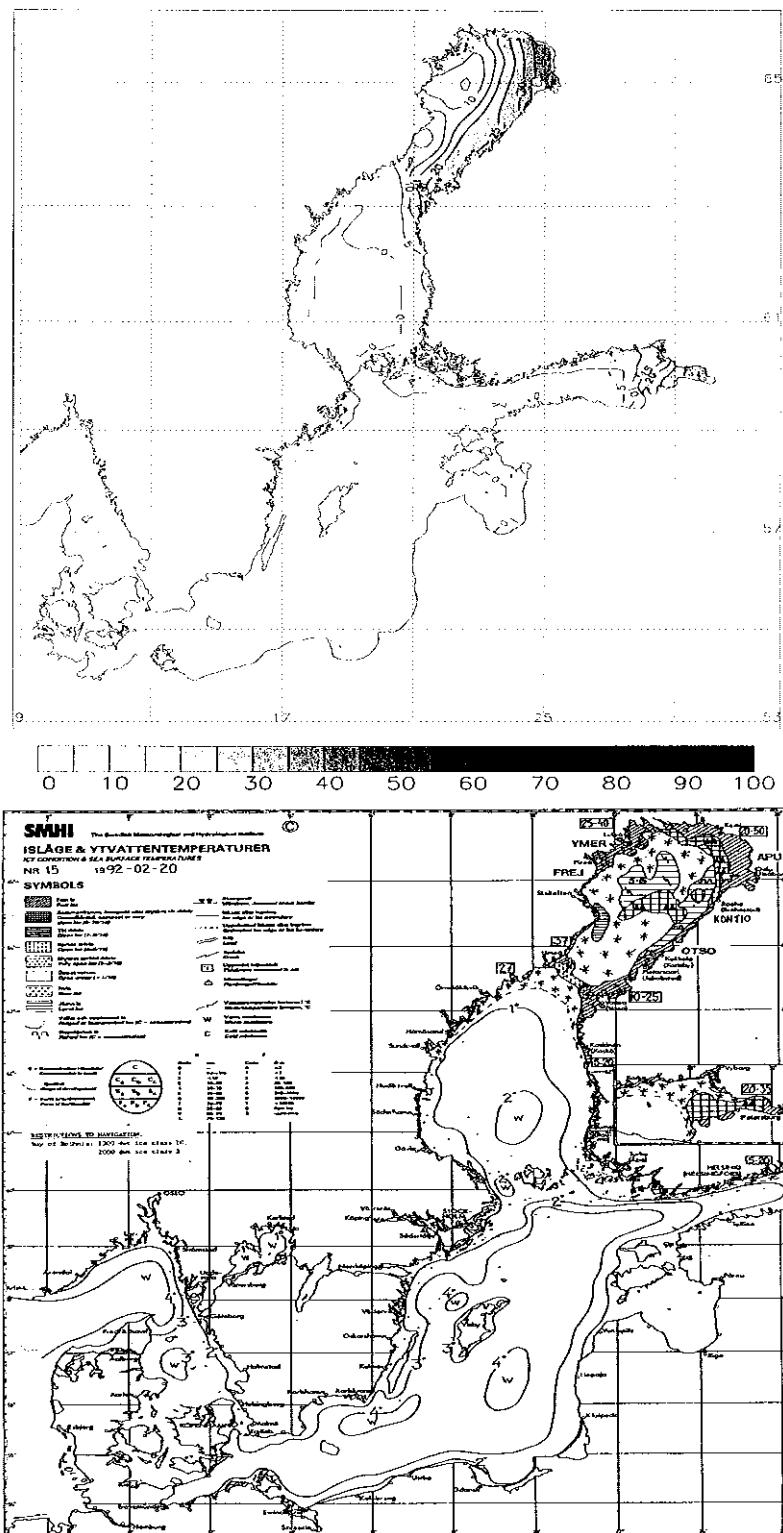
Figure 15: *Simulated ice thickness (in cm) on February 20 1992 (H1, upper panel), compared with the corresponding ice chart (lower) published by SMHI.*

timated and the area of newly formed ice in the Bothnian Bay is smaller compared with the observations (Fig.15). However, the overall agreement between simulated and observed snapshots is satisfactory.

Ice concentration and its temporal variability are dependent on the scale considered. Thus, model results are not directly comparable with observations. In ice charts ice concentration is mainly 100 % during the whole winter period. This is regarded as systematic bias due to the use of visual observations from ice breakers (Jari Haapala 2000; pers.comm.). Contrary, satellite data (SSM/I) yield a concentration between 70 and 100 %. These data tend to underestimate ice concentration, because SSM/I cannot differentiate between ice free water and melt ponds on the ice or flooded ice (Jari Haapala 2000; pers.comm.). As RCA underestimates surface winds, model results might overestimate ice concentration. In Fig.16, results of simulated ice concentration
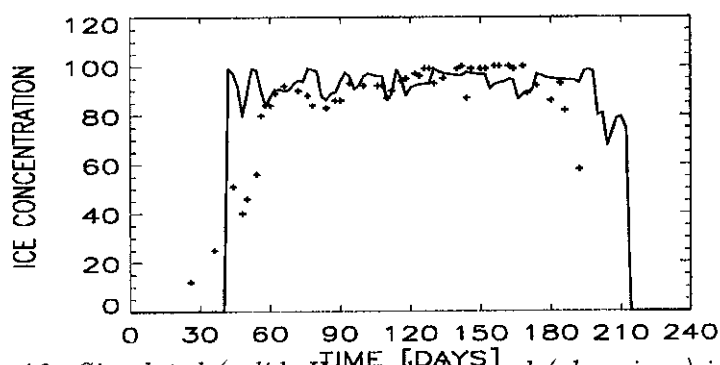
Figure 16: *Simulated (solid, H1) and observed (plus signs) ice concentration (in %) in the center of the Bay of Bothnia (65°N 27', 23°E 33') for the severe winter 1986/87. Plus signs are observed values based on SSM/I and ice chart data from the ice data bank for Baltic Sea climate studies (IDA, see Haapala et al. 1996). Time axis starts at October 1 1986.*

in the center of the Bothnian Bay from one ice season (1986/87) are compared with observations based on SSM/I and ice chart data from the ice data bank for Baltic Sea climate studies (IDA, see Haapala et al. 1996). In RCO ice concentration tends to grow too fast in autumn and tends to decrease too abruptly during the melting period in spring. In the presented example, ice concentration is simulated close to the maximum value, in agreement with the observations during the whole winter period. Contrary, during mild winters simulated ice concentration has higher variability between some 60, 70 % and 100 %. In summary, the analysis of hindcast results shows a high skill of the RCO ice model.

In scenario simulations the questions about the role of the ocean and about the uncertainty from the initial conditions arise (cf. spin-up discussion). If the seasonal heat storage in the ocean affects the sea ice season, a coupled ice-ocean model will be necessary to simulate inter-annual sea ice variability. In that case, however, inaccuracies of the ocean model (e.g. mixed layer depths) would affect ice model results, too. Otherwise, an off-line simulation performed with a ice model only would be suffi-

cient enough. There is also the question of model sensitivity of sea ice on sea surface salinity. As outlined earlier, two sensitivity experiments have been performed, one with underestimated seasonal thermocline depths (H5) and one with zero salinity (H4). The results show, that the ocean heat content affects ice extent, ice and even snow thickness tremendously (Fig.17). The ice-ocean heat flux is an important component in the
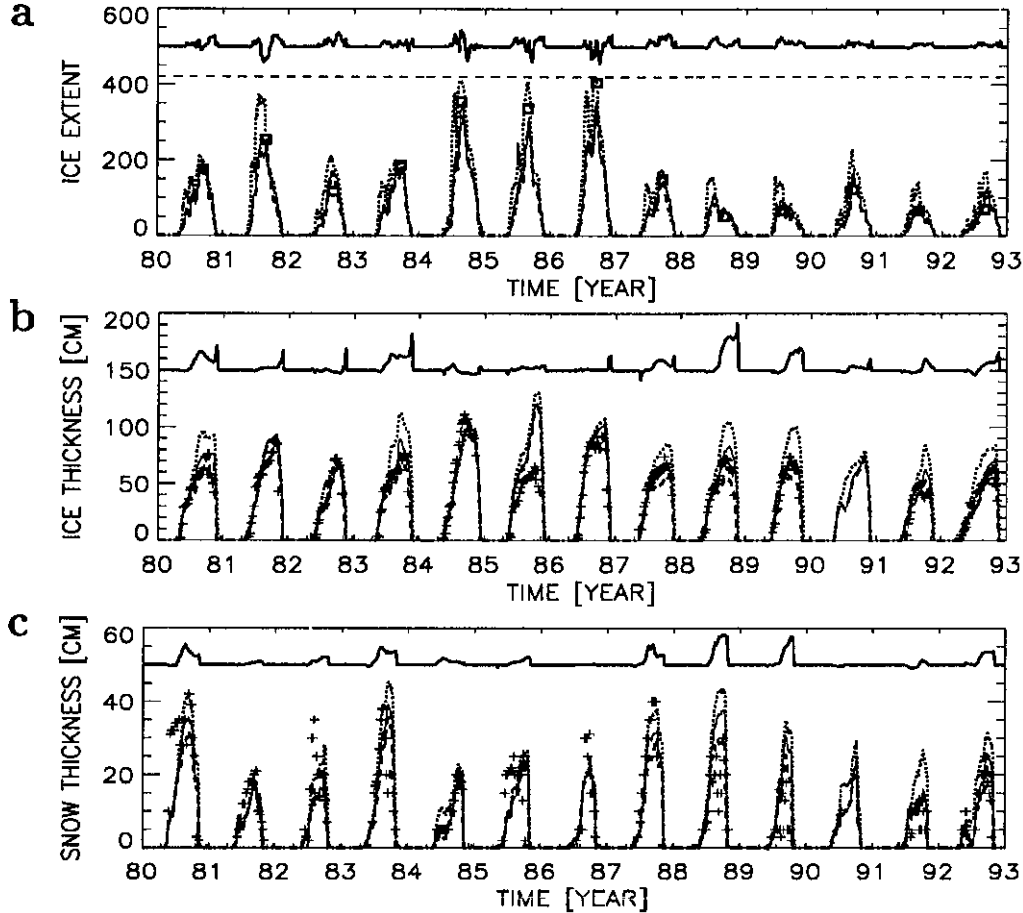
Figure 17: *As Fig.12, but thin solid lines denote the standard run (H1), thick dashed lines the sensitivity run with zero salinity (H4), thick dotted lines the sensitivity run with Richardson number dependent friction (H5), and thick solid lines (plotted with an offset) the difference between standard (H1) and zero salinity run (H4).*

balance of fluxes determining thermodynamical ice growth in autumn (see also Meier, 1999). Contrary, sea surface salinity is quite unimportant for Baltic Sea ice, because in areas with mean seasonal ice cover (Gulf of Bothnia and Gulf of Finland) salinity is low anyhow. Larger differences occur during severe winters, when ice covers also the southern Baltic with higher salinities.

6.3.2 Control and scenario simulations

In Fig.18, results of the control and scenario simulation are depicted for ice extent, ice and snow thickness at station Kemi in the northern Bothnian Bay using RCO-a (C1,
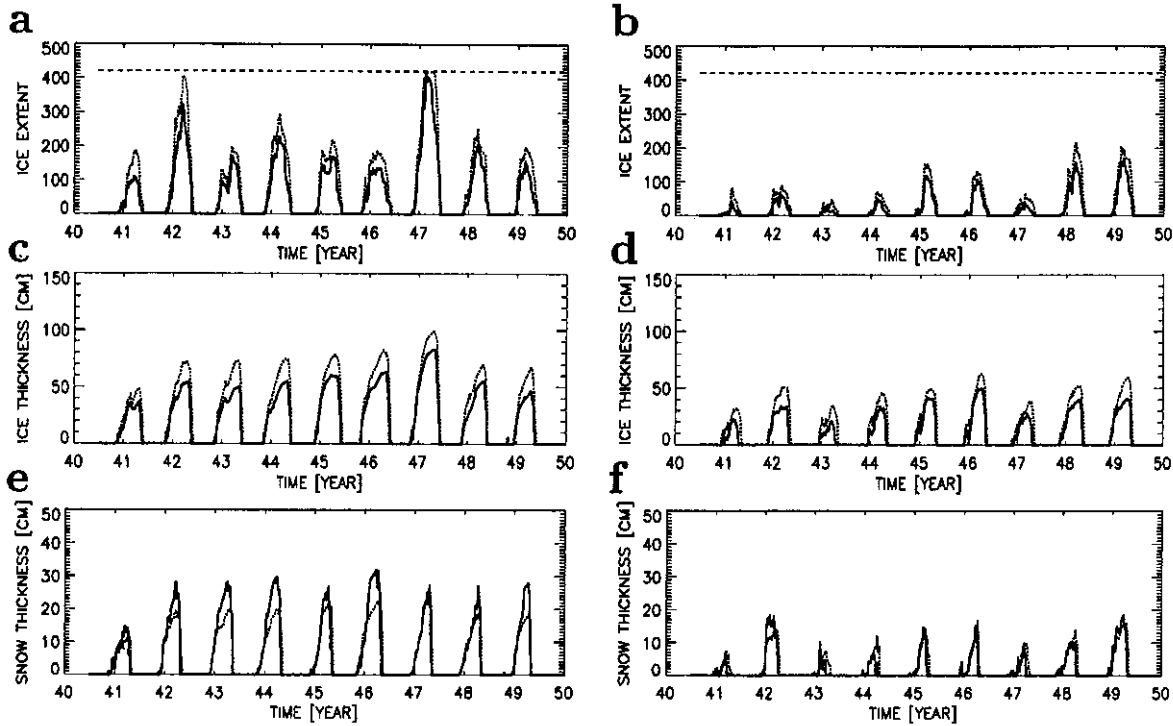
Figure 18: *Simulated ice covered area (in $10^9\,m^2$) for 9-year control run (a) and scenario run (b). Solid lines denote the standard run (C1, S1) and dotted the sensitivity run with icier climate conditions (C3, S3).*

S1) and RCO-b (C3, S3). Inter-annual variation of the ice winter severity is evident. Compared with the hindcast simulations (Fig.17), the control run (especially C3) lacks mild winters, but is within natural variability. In the control simulation there are two winters, when the maximum ice extent reaches (or almost reaches) $420 \times 10^3\,km^2$, which means that the Baltic Sea is totally frozen. Contrary, the scenario simulation shows a remarkable decrease in ice winter severity. However, ice is still formed every winter.

Ice and snow thickness at station Kemi are simulated realisticly in both control simulations. Snow thickness is slightly smaller than during the hindcast period and has smaller inter-annual variability. In the scenario run both quantities are very much reduced compared to the control run.

The statistics of maximum ice extent, maximum annual ice thickness in the Bothnian Bay center, and number of ice days at Kemi in the Bay of Bothnia and at Kotka in the Gulf of Finland (see Fig.1) are listed in Tab.7. The mean maximum ice extent in the control run using RCO-a (C1) of $210 \cdot 10^9\,m^2$ is very close to the observed long-term (1720-1996) mean value of $217 \cdot 10^9\,m^2$ (Tinz 1996). Also standard deviations are close, but there are no mild winters in RCO, most likely due to the short integration period. Minimum, maximum and standard deviation in RCO-a are $110 \cdot 10^9\,m^2$, $406 \cdot 10^9\,m^2$ and $96 \cdot 10^9\,m^2$, respectively. Corresponding numbers from the 277-year observed record are $52 \cdot 10^9\,m^2$, $420 \cdot 10^9\,m^2$ and $114 \cdot 10^9\,m^2$, respectively (Tinz 1996). In the scenario run using RCO-a (RCO-b) mean maximum ice extent is reduced by 61 (55) % and mean maximum annual ice thickness in the Bothnian Bay by 46 (39) %. The mean ice

31

Control run	RCO-a			RCO-b			HIM		
Variable	min	mean	max	min	mean	max	min	mean	max
Ice extent ($10^9\,m^2$)	110	210	406	181	261	419	190	290	420
Ice thickness (cm)	35	54	81	48	71	96	32	49	66
Ice season at Kemi (day)	154	191	214	176	207	232	179	199	223
Ice season at Kotka (day)	118	163	206	144	176	196	144	173	202
Scenario run	RCO-a			RCO-b			HIM		
Variable	min	mean	max	min	mean	max	min	mean	max
Ice extent ($10^9\,m^2$)	16	82	168	45	117	217	50	190	270
Ice thickness (cm)	11	29	47	28	43	60	11	27	39
Ice season at Kemi (day)	126	151	178	148	168	190	137	164	183
Ice season at Kotka (day)	18	89	142	60	117	160	87	131	169

Table 7: *Comparison between two different RCO versions (RCO-a and RCO-b) and HIM (the Helsinki Ice Model; Haapala et al. 2000) in control and scenario simulation. Minimum, mean and maximum values are tabulated of maximum annual ice extent, maximum annual ice thickness in the center of the Bay of Bothnia ($65°N\,27'$, $23°E\,33'$) and number of ice days at Kemi in the Bay of Bothnia ($65°N\,39.8'$, $24°E\,31.4'$; see Fig.1) and Kotka in the Gulf of Finland ($60°N\,27.3'$, $26°E\,57.2'$; see Fig.1).*

seasons at Kemi and Kotka are 21 (19) % and 45 (34) % shorter, respectively. Overall, the numbers of relative change are quite similar in both ensembles.

As shown in the ice atlas by SMHI and FIMR (1982), the statistic of observed maximum ice extent of the investigated period 1964-1979 is quite similar to the long-term mean. Hence, also statistics of other variables of the ice atlas are considered as climatological mean conditions of the Baltic Sea ice season. A comparison of results of the standard control run (C1) with ice atlas data shows, that mean time evolution of ice cover, mean maximum annual ice thickness, and mean number of ice days fit quite well with the observations (Fig.19a, Fig.20 and Fig.21).

The maximum of mean time evolution of ice cover and variability of the control run are close to the observations (Fig.19a). However, the maximum is shifted in time by about 18 days and, consequently, the simulated mean melting date is delayed. This result does not occur in hindcast simulations (Tab.6), but is also reported by Rummukainen et al. (2000) from results of the RCA1 run coupled with a different, horizontally integrated ice-ocean model for the Baltic Sea. The discrepancy may be partly explained by differences in defining ice cover. The observational estimate is based on digitized ice charts for 1963-1979, in which each $0.25 \times 0.5°$ grid box is classified as ice when the subjectively analyzed ice concentration is at least 10%. Contrary, the size of a model grid box is only $0.1 \times 0.2°$ and there is no ice concentration threshold. In addition, the spring cold bias in the GCM driving the regional model may contribute to the shifted ice season.

In Fig.20, the mean maximum annual ice thickness of the standard control run (C1) is compared with observations. Simulated maximum ice thickness increases from 20 cm
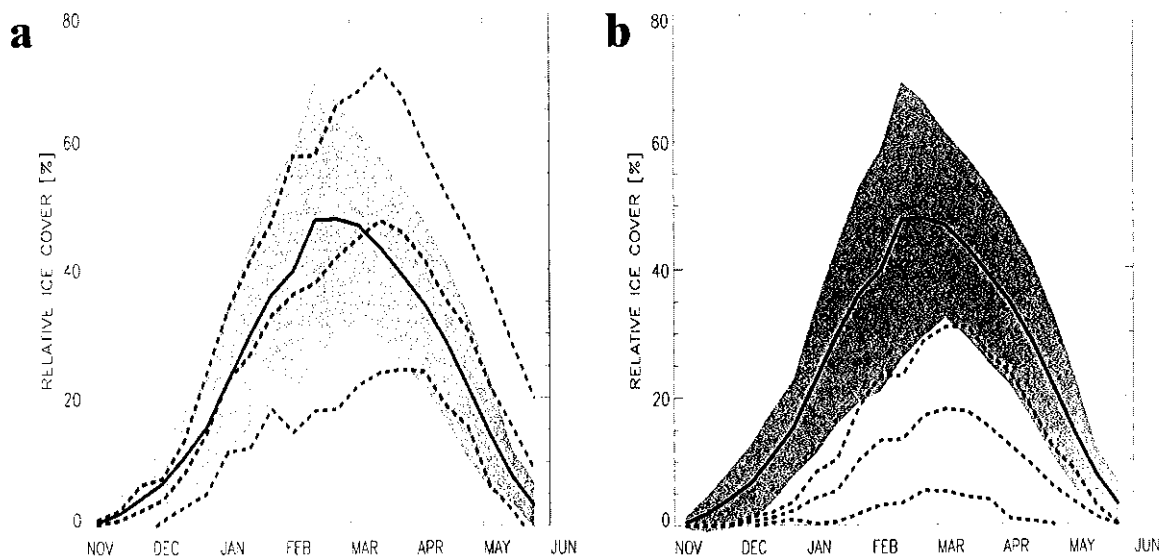
Figure 19: *Frequency distribution of Baltic Sea ice area. The solid curve denotes the observed mean time evolution of ice area for the period 1963/64-1978/79 (SMHI and FIMR 1982) and the shaded area shows the range of variability defined by added or subtracted standard deviations. Correspondingly, the dotted curves denote the simulated mean time evolution of relative ice cover and the range of variability for the control run (C1) in (a) and for the scenario run (S1) in (b).*

in the Åland Sea, to 20-30 cm in the Bothnian Sea, to 40-50 cm in the Bothnian Bay, and to more than 50 cm in the fast ice zone of the northern Bothnian Bay. Contrary, observed maximum ice thickness is higher by about 10 cm in the center of the Bothnian Bay and by about 20 cm in the northern fast ice zone.

In Fig.21, the mean number of ice days (all cases) is depicted. In simulation and observations the mean ice season in the central Bothnian Sea is about 50 days long. In the central Bothnian Bay the ice season lasts about 130 days and in the northern fast ice zone more than 190 days. The agreement between control run and observations is satisfactory.

In Fig.19b, the mean time evolution of ice cover for the scenario run (S1) is shown. Mean ice cover is very much reduced and the ice season length is shorter than in the control run and in observations.

For two more variables, i.e., mean maximum annual ice thickness and mean number of ice days (all cases), the changes between scenario and control run are shown in Fig.22 and Fig.23, respectively. As in Tab.7, the changes are calculated for both versions RCO-a (S1-C1) and RCO-b (S3-C3), to estimate uncertainties. In the central Bothnian Bay mean maximum annual ice thickness is reduced in the scenario run by 30 to 35 cm using RCO-b and by 20 to 25 cm using RCO-a. The difference of the two changes is depicted in Fig.24a. Maximum differences in the Gulfs (changes in the Baltic proper are insignificant) of about 10 to 15 cm are located in the central Bothnian Bay and in

Mean maximum annual ice thickness, in cm
Medelvärdet av den maximala istjockleken för de olika åren, i cm
Keskimääräinen vuotuinen maksimipaksuus (cm)
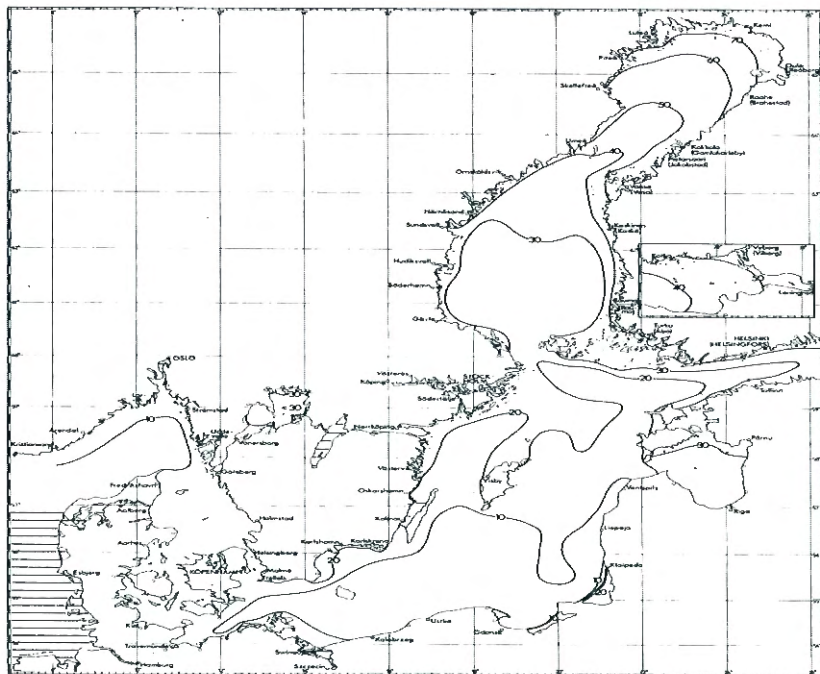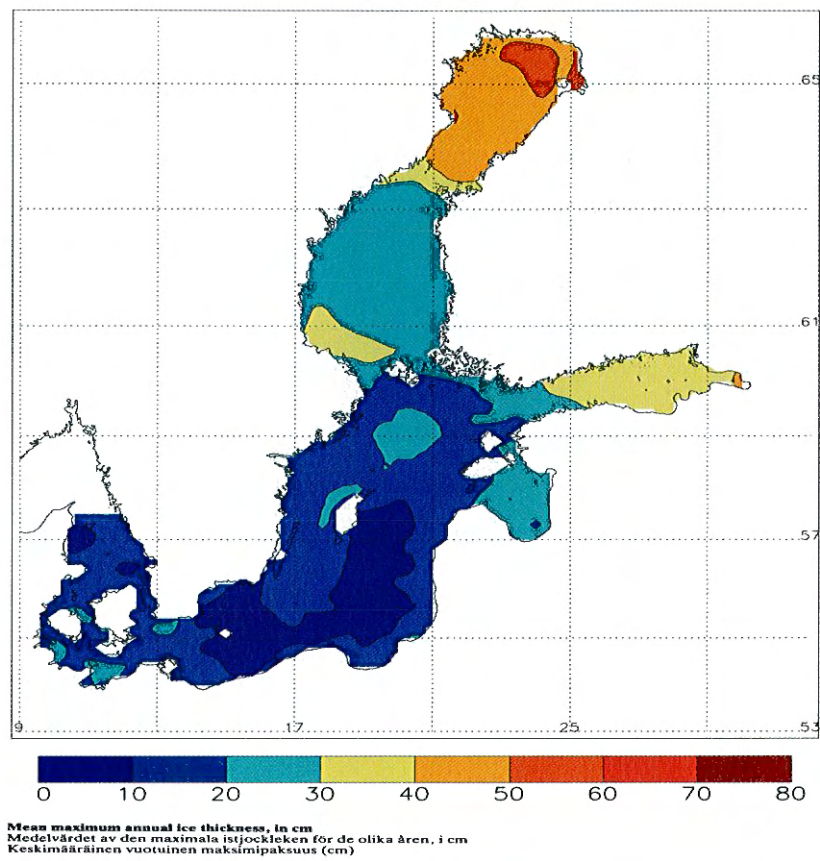
Figure 20: *Mean maximum annual ice thickness (in cm) from control run C1 (upper panel) and observations (lower) by SMHI and FIMR (1982).*

34
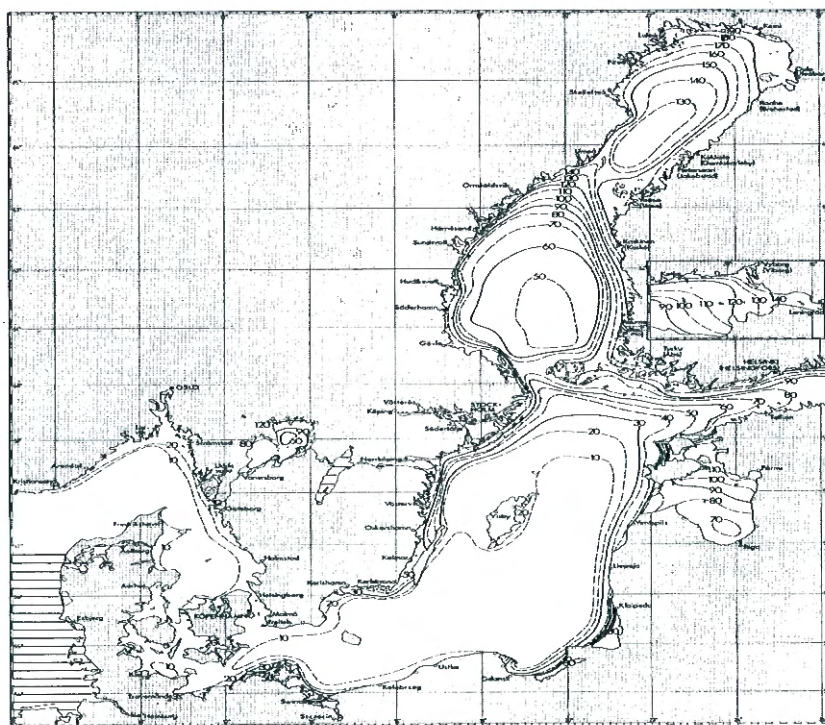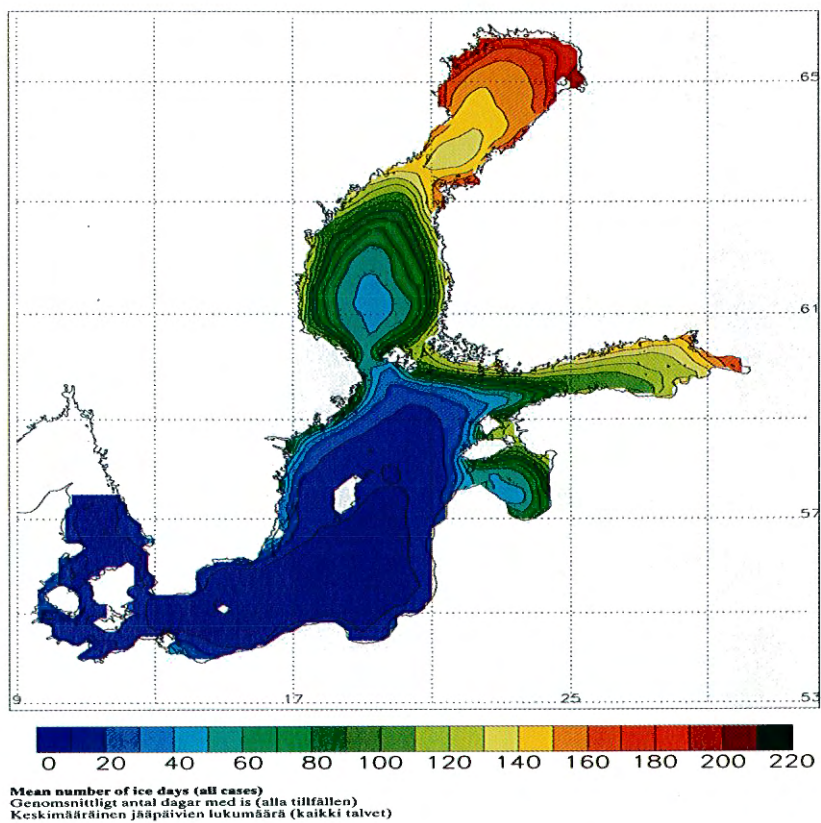
Figure 21: *Mean number of ice days (all cases) from control run C1 (upper panel) and observations (lower) by SMHI and FIMR (1982).*

35
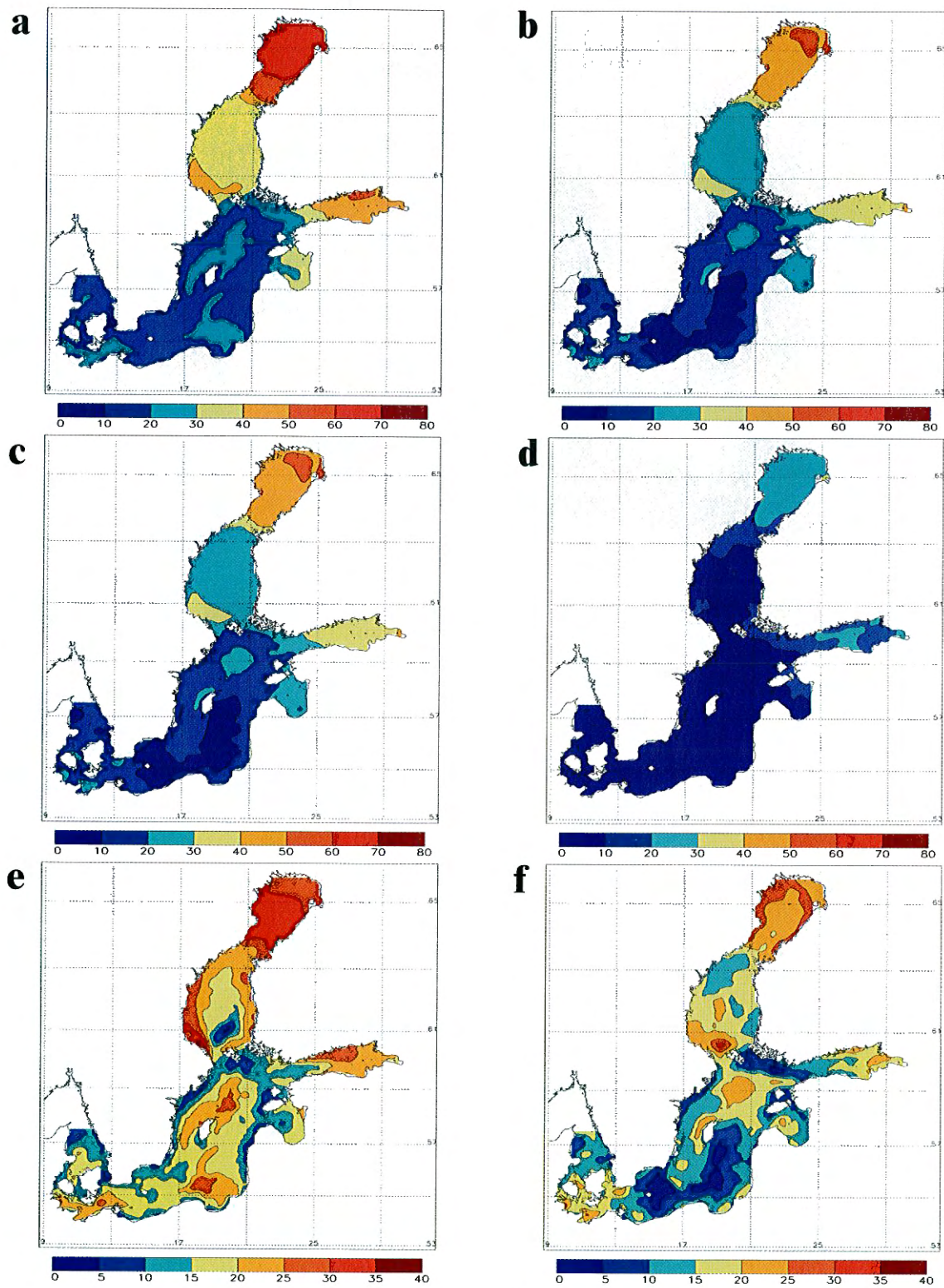
Figure 22: *Mean maximum annual ice thickness (in cm) for control run (a,b), scenario run (c,d) and change (e,f). The left panels (a,c,e) are calculated with RCO-b (C3, S3) and the right panels (b,d,f) with RCO-a (C1, S1).*

36
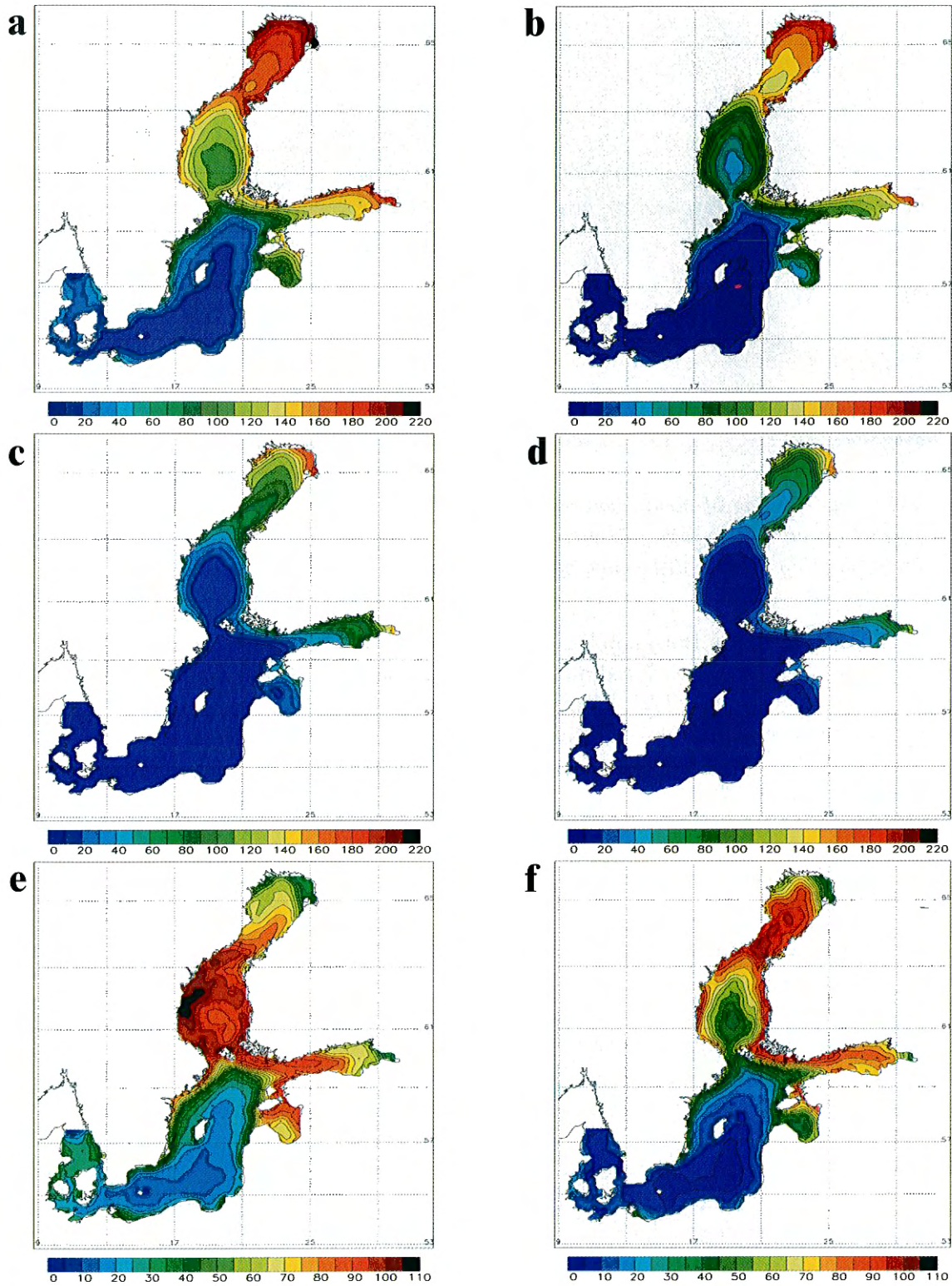
Figure 23: *Mean number of ice days (all cases) for control run (a,b), scenario run (c,d) and change (e,f). The left panels (a,c,e) are calculated with RCO-b (C3, S3) and the right panels (b,d,f) with RCO-a (C1, S1).*

37
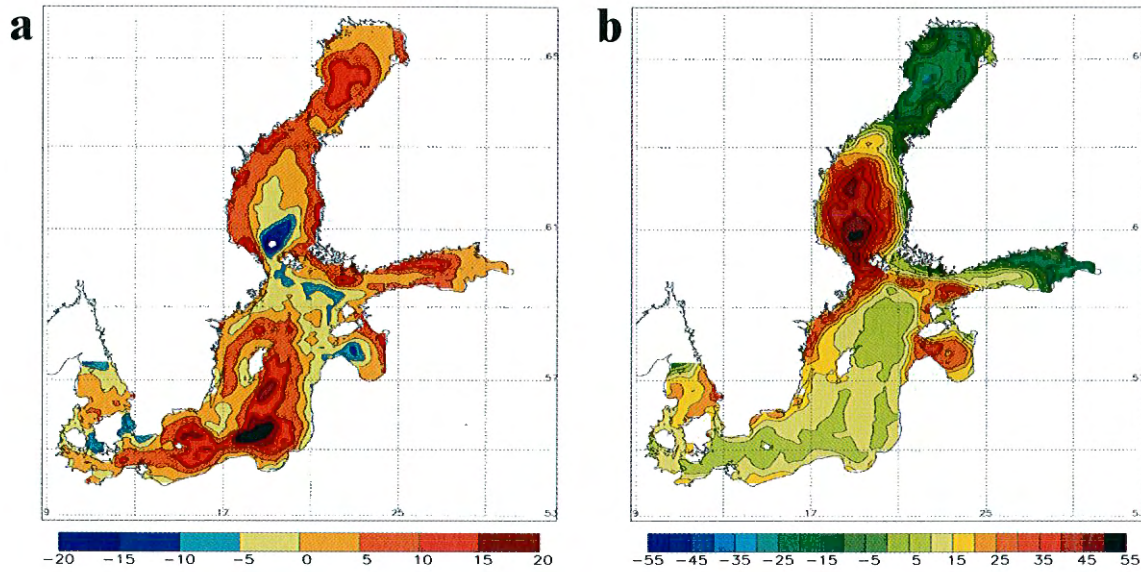
Figure 24: *(a) Change of mean maximum annual ice thickness (in cm) simulated with RCO-b (S3 minus C3) minus the corresponding change using RCO-a (S1 minus C1). (b) Corresponding change difference of mean number of ice days (all cases).*

some coastal areas of the Bothnian Sea and northern Gulf of Finland. The mean number of ice days in RCO-b is reduced most in the Bothnian Sea (because of decreased ice extent) by about 85 to 110 days. Contrary, in RCO-a the smaller maximum change of ice days of about 85 to 100 days is shifted to the North with location in the southern Bothnian Bay. The largest difference of the two changes is found in the Bothnian Sea of more than 40 days (Fig.24b).

6.4   Sea level

The focus of the analysis is on 9-year mean SSH (Fig.25) and 9-year mean maximum annual SSH (Fig.26). The latter is regarded as a measure of extreme sea level events.
 In the hindcast run mean SSH and SSH extremes are calculated for the period 1980 until 1989. The mean sea level increases from Kattegat to the Gulf of Bothnia and to the Gulf of Finland with about 25 to 35 cm (Fig.25a). The slope is caused by freshwater supply of rivers located mainly in the northern and eastern parts of the Baltic Sea. In addition, mean wind speed from south-westerly directions contributes to the slope (Meier 1999). In Fig.25a, values of the mean sea level of selected tide gauge positions in comparison to the geoid solution of Ekman and Mäkinen (1996) are shown additionally. Ekman and Mäkinen designed a consistent height system for comparisons between geodesy and oceanography for the Baltic Sea area and computed mean sea surface topography geodetically in this height system at 42 reliable long-term sea level stations, connected by high-precision levelings, along the coasts of the Baltic Sea, the Kattegat, the Skagerrak and the adjacent part of the North Sea. Some stations are selected here. These are from North to South in Finland Kemi-Ajos, Oulu, Pietarsaari, Maentyluoto, Helsinki, Hamina, in Sweden Furuögrund, Ratan, Forsmark, Landsort, Klagshamn,

38
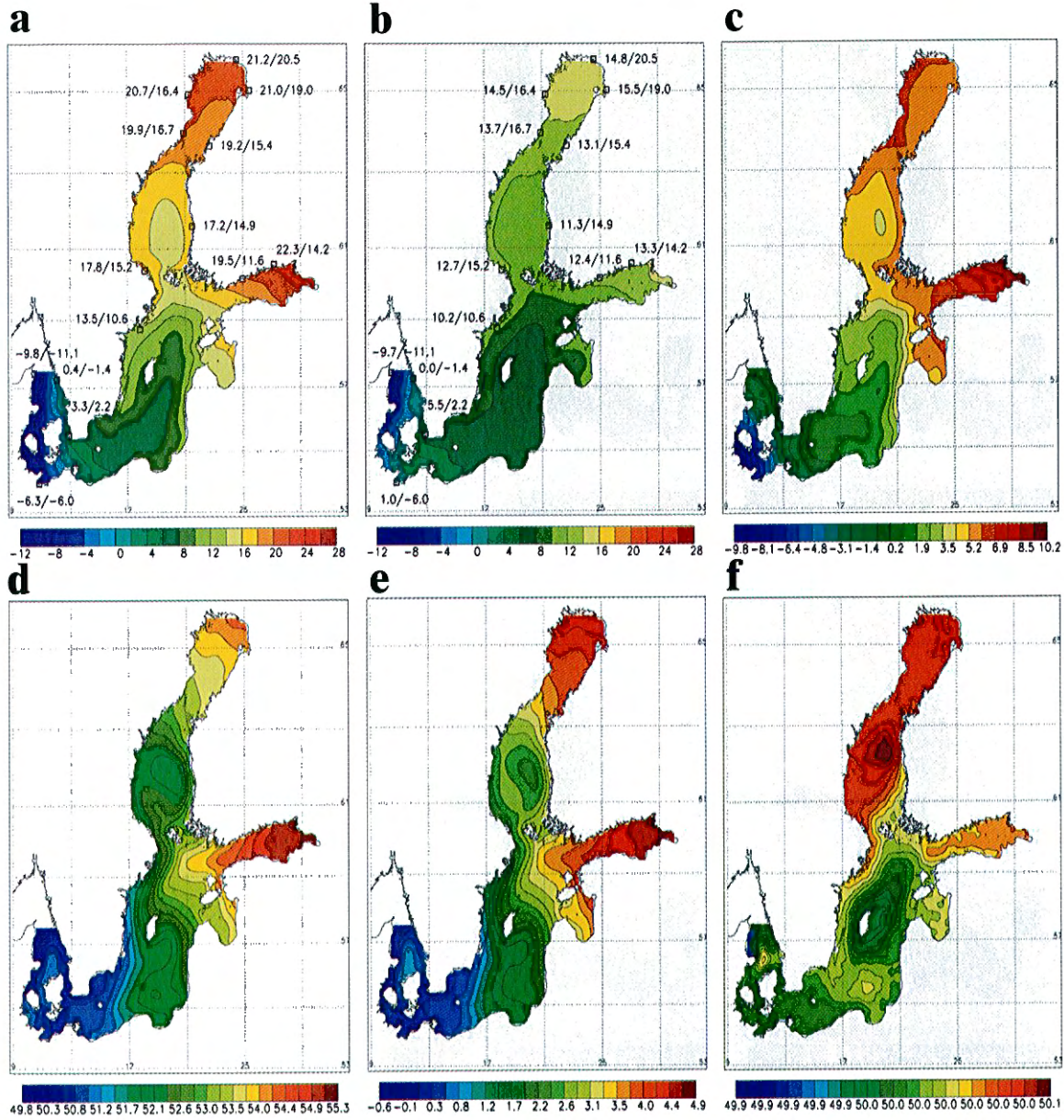
Figure 25: *9-year mean sea surface height (in cm): (a) hindcast run (H1), (b) control run (C1), (c) hindcast minus control run (H1 minus C1), (d) scenario with global mean sea level rise of 50 cm minus control run (S5 minus C1), (e) standard scenario minus control run (S1 minus C1), (f) difference between the scenarios (S5 minus S1). Note the different color bars. The numbers in (a) and (b) at selected tide gauge positions indicate model results (left) and geoid solutions of Ekman and Mäkinen (1996) (right).*

Ringhals, in Denmark Frederikshavn, and in Germany Travemünde. There is a general agreement between mean SSH in RCO and the geodetic result. Larger differences occur only in the Gulf of Finland. The reason might be an overestimation of mean wind speed in the atmospheric data set. As RCO is used with the coarse horizontal resolution of 6 nm, the topography of the Danish Straits is not well represented in the model and had to be changed artificially (broadening of the strait width). Especially, volume transports through the Sound cannot be correct. Nevertheless, observed and
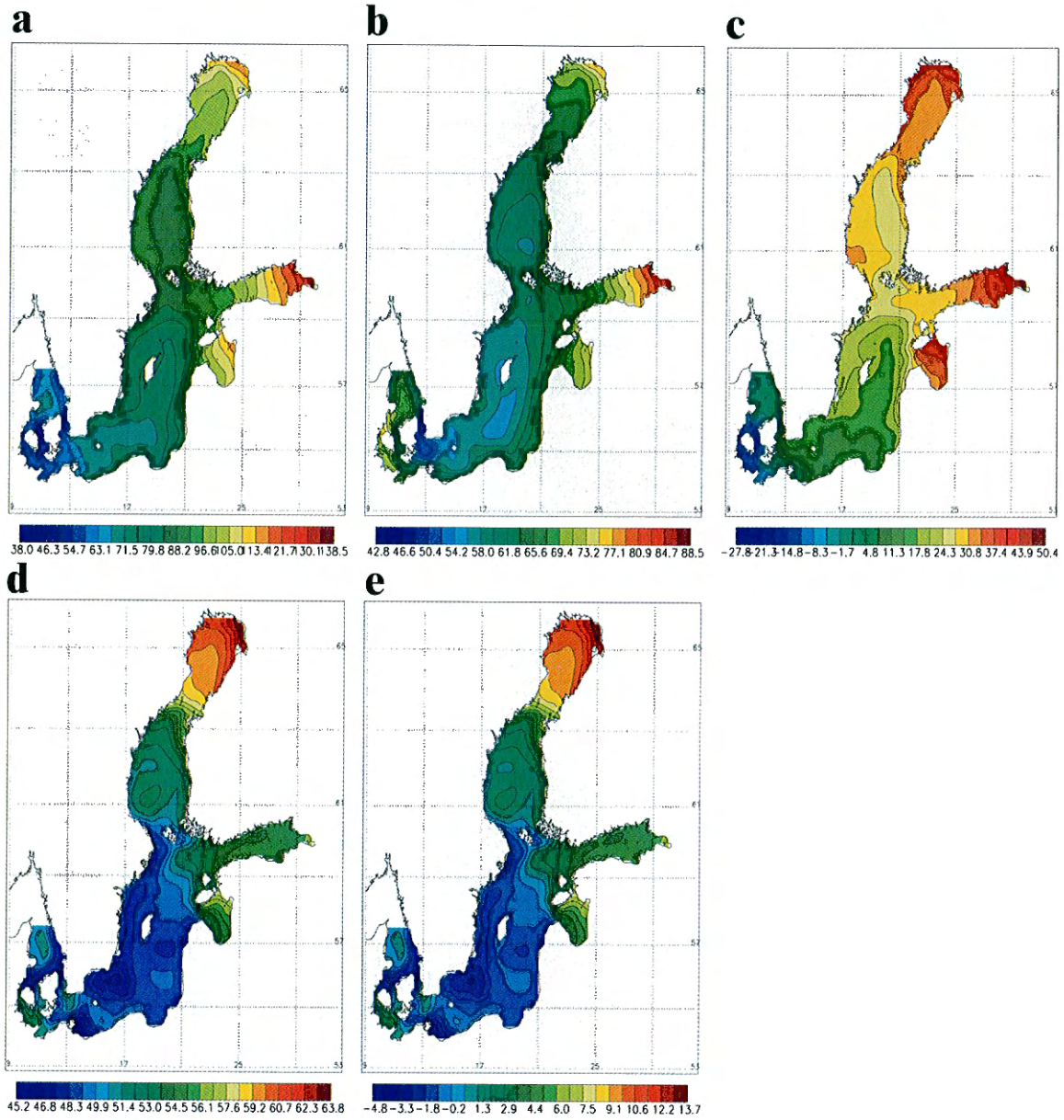
Figure 26: *9-year mean maximum annual sea surface height (in cm): (a) hindcast run (H1), (b) control run (C1), (c) hindcast minus control run (H1 minus C1), (d) scenario with global mean sea level rise of 50 cm minus control run (S5 minus C1), (e) standard scenario minus control run (S1 minus C1). Note the different color bars.*

simulated sea surface heights are not very different in the Danish Strait region.

SSH differences between hindcast (H1) and control run (C1) are quite large with about $\pm 10\,cm$ (Fig.25c), because in the control run the upper layer salinity shifts to lower salinity due to higher runoff than observed (Tab.3). In addition, wind speeds in the control run are lower.

In general, the mean SSH change in the Baltic Sea between scenario (S5) and control run (C1) follows the change at the open boundaries, i.e., the mean sea level change

40

in the North Sea (Fig.25d). In the scenario run S5 a global mean SSH rise of 50 cm between the two time slices is assumed. Thus, the overall SSH rise in the Baltic Sea is also 50 cm. In the Gulf of Finland and in the Gulf of Bothnia an additional increase of about 5 cm is found. This is related to a small increase in the mean wind speed and higher runoff in the scenario run compared to the control run (Fig.25e). The differences between the two scenarios S5 and S1 are 50 cm with local deviations smaller than 0.1 cm (Fig.25f).

In the hindcast run (H1) maxima in mean maximum annual SSH are found in the Gulf of Finland and Gulf of Bothnia and minima in the Belt Sea (Fig.26a). It is assumed, that extremes in the western Baltic (e.g. Arkona Basin, Belt Sea, etc.) are underestimated, because the widths of the Danish Straits have been increased artificially. Maximum extremes in the hindcast run (H1) are higher in the Gulf of Bothnia with about 37 cm and in the Gulf of Finland with about 47 cm than in the control run (C1) (Fig.26b,c). Correspondingly, minimum extremes in the Belt Sea are smaller by about 19 cm. The differences between control and hindcast run are smallest in Kattegat, because the same sea level observations are used in both runs.

Due to the same reason, in all scenario runs the variability is not changed at the open boundaries. Approximately, changes of mean maximum annual SSH are similar than changes of mean SSH, i.e., 50 cm higher extremes (Fig.26d). However, the changes in the Gulf of Finland (about 57 cm) and in the Gulf of Bothnia (about 63 cm) are higher. These increases might be explained by higher wind speed during storm events.

7 Discussion

For multi-year simulations of the Baltic Sea, it is important to simulate vertical stratification without erosion of the halocline. No systematic bias is evident in RCO in the deep layer during the stagnation period and only a small bias in the upper layer. However, it should be noted, that the stagnation period 1976-1992 is a very special one. If satisfying model results can be obtained also during periods with many salt water inflows, requires further investigation.

River runoff calculated from the RCA control run is 32.6 % higher than observed runoff. This causes salinity in the upper layer of the Baltic Sea to drift by about -0.5 to -0.8 psu per 10 years. Thus, longer integrations cannot be performed with runoff calculated from RCA precipitation directly. The so-called "δ-change" technique needs to be applied for the time being, i.e., river runoff is calculated from observations plus the relative change of scenario minus control run.

High wind speeds in RCA (and other coarse resolution atmosphere models, e.g. ERA) are underestimated affecting inte alia diffusivity. Salinity differences between control and hindcast run are largest in the upper halocline. More realistic wind fields might be obtained with higher resolution in RCA.

Another problem concerning scenarios of salinity arises from the time slice technique, i.e., the problem with spin-up of the future scenario experiment. Pending of long coupled atmosphere-ocean transient runs based on regional models (see discussion of spin-up strategy above), salinity is treated as uncertainty in this report. In a 90-year spin-up experiment (using 9 years of atmospheric forcing data repeatedly 10 times) a future extreme case has been calculated with the assumption, that no salt water inflow occurs. The sub-cycling technique has been used also by Omstedt et al. (2000), but they assumed, that one inflow event of the strength of the one from January 1993 occurs every 10 years. In addition, they used for their 100-year PROBE-Baltic run the absolute runoff of the RCA0 scenario, i.e., 21,000 m^3/s in the 10-year mean, which is very high compared to present-day climate plus expected changes (Tab.3). Due to different assumptions there long-term experiments cannot be compared, although they are astonishingly similar. However, both results might be essentially biased by model shortcomings. According to Omstedt et al. (2000), the PROBE-Baltic model overestimates bottom salinities during the inflow event. In both models the same coarse deep water mixing parameterization (inverse proportional to the Brunt-Väisälä frequency) is applied, which does not include any wind effect. To the authors opinion, it is too early to judge about the predictability of salinity on such long time scales by any available Baltic Sea model (process-oriented or 3D).

Annual mean and seasonal mean SST changes between scenario and control runs are larger than the uncertainty due to unknown salinity. However, SST changes are not totally insensitive to this uncertainty (largest in summer with $-0.5\,°C$ in the areal mean). Contrary, the ice model is not very sensitive on changes in sea surface salinity. Thus, the climate change signal in ice variables is not biased by salinity uncertainties.

For the scenario time slice, it is assumed, that sea level variability in Kattegat will not change in future. The SST and sea ice results shown here are independent of the used period for sea level data at the open boundaries in Kattegat. This was the result of a sensitivity experiment of the scenario run forced by sea level data from the shifted period 1985-1995 (not shown). Another sensitivity experiment revealed, that also the predicted global mean sea level rise of the order of about 50 cm, as reported from many GCMs, does not affect simulated SSTs or sea ice in the Baltic. Due to 50 cm increased sea level in Kattegat an initial "shock" occurs and salt water enters the western Baltic Sea. However, after about one or two years the inflowed salt water is diluted and stratification in the scenario run with global mean sea level rise is almost identical to the one without increased sea level. Also the boundary conditions for temperature and salinity in Kattegat are assumed to be relatively unimportant in the time slice experiments, because the Baltic Sea is closed thermodynamically (Meier 2000; Omstedt and Rutgersson 2000) and because only major inflows are sensitive on surface layer salinity outside the model domain, if the incoming volume is larger than the Kattegat surface layer volume (see Meier et al. 1999).

In this report two different versions of RCO, RCO-a and RCO-b, have been used to perform scenario simulations. From both, a first guess of uncertainties due to unknown

heat flux parameterizations is possible. Although it has been shown that RCO-a performs better in hindcast simulations using the SMHI database as atmospheric forcing, scenario results derived with RCO-b are regarded realistic as well. Important differences between the two versions are related to the cloud parameterization in the shortwave and incoming longwave radiation (Tab.2). It is assumed, that the higher sensitivity of the radiative flux parameterizations on total cloudiness might contribute to compensate errors in the SMHI database. Most of the observational stations in the database are located on land making a bias likely. On the other hand, RCA1 model results with boundary data from HadCM2 are biased as well (e.g., summer temperature cold bias). Further investigations are necessary to find appropriate heat flux parameterizations in hindcast experiments using independent observational data sets.

Differences in the versions RCO-a and RCO-b affect mainly sea ice results because the annual ice cover is very sensitive on short and longwave radiation in spring and autumn, respectively. In Tab.5 area averaged SST changes simulated with the two model versions are compared. Differences between the changes are relatively small (largest in autumn with $0.23\,^{\circ}C$).

The results of RCO have been compared also with those of the Helsinki ice model (HIM) by Haapala and Leppäranta (1996) and Haapala (2000) using the same RCA1 atmospheric forcing (Haapala et al. 2000). In general, climate change of the ice phase is simulated similar with both model systems, although they are quite different. With respect to ice extent, the Helsinki model is closer to the icier version RCO-b (Tab.7). In all three ensembles it is found, that ice extent in the scenario run decreased dramatic. Ice could still be found in the Bothnian Bay in every simulated year. However, in detail there are differences (see Tab.7). In the scenario run using RCO-a (RCO-b) [HIM] mean maximum ice extent is reduced by 61 (55) [34] % and mean maximum annual ice thickness in the Bothnian Bay by 46 (39) [45]%. The mean ice seasons at Kemi and Kotka are 21 (19) [18] % and 45 (34) [25] % shorter, respectively. Absolute changes of mean maximum ice extent are 128 (144) [100] $\times 10^9\,m^2$ showing a different sensitivity of the models on simulated climate change.

Contrary, Omstedt et al. (2000) found that almost no ice occur during 3 out of 10 winters in the scenario run. Their results are obtained using downscaling simulations of an earlier RCA version (RCA0, see Räisänen et al. 1999). Indeed, in that scenario experiment surface air temperature over the Baltic Sea increased by 3-5 $^{\circ}C$ in the annual mean and 4-11 $^{\circ}C$ in December-February (Fig.3 by Räisänen et al. 1999), which is much higher than in the scenario presented here (based on RCA1). However, Omstedt et al. (2000) concluded from earlier sensitivity experiments, using the process oriented PROBE-Baltic model, that with an air temperature increase of $+3^{\circ}C$ (reference period: 1981-1995) the maximum annual extent of ice could be expected to become zero during 1 out of 15 winters. Here, the area mean winter air temperature change over the Baltic Sea is of comparable magnitude with $3.5\,^{\circ}C$. None of the 9(10) winters in the scenario experiments gets completely ice-free. If that will be the case in a RCO sensitivity experiment for the period 1981-1995 including several mild winters, is an open question. However, based on the newest scenario results one cannot conclude,

that the Bothnian Bay will be ice-free during some winters in 100 years. As the time slice experiments are too short and as the control run does not include mild winters, one can also not conclude the contrary, i.e., there will be sea ice in the Baltic every winter in 100 years.

As consequence of increasing global mean temperature, the global mean sea level increases due to thermical expansion and melting glaciers. If all continental ice melts, the global mean sea level would rise by about 50 cm. Correspondingly, the melting of the ice on Greenland and on Antarctica would result in 7 m and 61 m higher sea level in the world ocean, respectively. A summary of available scenario results of different GCMs gives an average of 50 cm global mean sea level rise in 100 years with a range of 10-90 cm. Thereby, thermical expansion contributes to the global rise with 60 % and melting of continental glaciers together with some other smaller factors like permafrost melting, sediment transport into the ocean, changes in ground-water level, etc. with 40 %. It is assumed, that the huge ice mass of Greenland and Antarctica is too inert and will not change during the next 100 years. In the present report a global mean sea level rise of 50 cm is assumed to occur also locally in the North Sea. Indeed, there is evidence from observations that climate change may cause increasing sea levels. Ekman (1999) analyzed the world's longest sea level record from Stockholm and found, that the general climatic rise of sea level has increased significantly from 0.0 mm/year during the end of the Little Ice Age, to about 1.0 mm/year during the past century. However, this number is smaller than the apparent land uplift, i.e., the uplift relative to the mean sea level (1892-1991), in the central and northern Baltic Sea. Ekman (1996) found the maximum apparent land uplift of 9 mm/year in the Bothnian Bay and 0 mm/year in Kattegat. The standard error is typically 0.2 mm/year. Thus, global mean sea level rise affects the Gulf of Bothnia less than Kattegat, Danish Straits and the western Baltic Sea.

Like in other studies of simulated climate change, the results might be affected very much by several uncertainties not discussed in this report. These are internal variability (the experiments are quite short), the assumption of greenhouse gas emission scenarios and model errors of HadCM2 and RCA (a number of ensemble simulations is necessary). For a discussion on internal variability the reader is referred to Räisänen (1999). Model errors of HadCM2 and RCA are discussed further by Räisänen and Döscher (1999) and Rummukainen et al. (2000).

8 Conclusions

Two prerequisites are necessary to perform climate change scenarios for the Baltic Sea using 3D coupled ice-ocean models, i.e., climate models with sufficient performance in long-term simulations and atmospheric forcing data of future climate.

Since autumn 1999 first results of decade-long integrations have been reported (e.g. Meier 1999; Schrum et al. 2000). This enormous effort was possible, because avail-

able computer resources have increased and more physically correct parameterizations of unresolved processes have been developed. Explicitly prescribed mixing is larger than implicit included numerical diffusion in solving the discretized primitive equations within 3D models. Results of a hindcast simulation for the period 1980-93 using the coupled ice-ocean model RCO (Rossby Centre regional ocean climate model) show, that erosion of the halocline is avoided and salinity in the Baltic proper deep water decreases as observed. Improved surface heat flux and mixing parameterizations enable realistic simulation of SST in present-day climate.

Recently, atmosphere scenarios from regional climate models became available for the Baltic Sea catchment area. The RCA (Rossby Centre regional atmosphere climate) model was used to improve the much coarser results from the coupled ocean-atmosphere GCM model HadCM2 through dynamical downscaling (Rummukainen et al. 2000; Räisänen et al. 2000).

As necessary prerequisites are fulfilled, in this study two 9-year time slice simulations representing control (pre-industrial) and scenario (future) climate could be performed. Despite of mainly GCM caused biases, the control run gives realistic present-day climate. Thus, the scenario run is regarded as possible projection of how future might develop based upon a set of internally consistent assumptions.

The main conclusions may be summarized as follows:

- Although initial conditions for the future time slice are unknown and salinity is treated as uncertainty only, it is shown, that calculated SST changes are significant in that sense, that the signal is larger than the respective uncertainty. Although salinity after 100 years of spin-up (assuming that no salt water inflow occurs in future) is much reduced compared with present-day conditions, the weak haline stratification is able to limit the seasonal thermocline sufficiently, so that SST differences between scenarios initialized with present-day climate conditions and with spin-up results after 90 years are relatively small. Salinity in the Baltic Sea cannot decrease to any small value, because continuously inflowing water from the North Sea compensate always diffusion across the halocline, independent of meteorological conditions forcing major salt water inflows.

- The seasonal heat content affects ice season. Thus, a coupled ice-ocean model should be used to simulate Baltic Sea ice in changing climate.

- The sensitivity of sea ice in the Baltic Sea on salinity is relatively small. Thus, the uncertainty of future initial salinity conditions does not affect ice scenarios.

- The change of mean maximum annual ice thickness is larger in the icier RCO version and the maximum change of mean number of ice days shifts from the Bothnian Sea in the icier RCO version towards the southern Bothnian Bay in the milder RCO version. Thus, model dependent uncertainties may affect simulated climate changes, which cannot be neglected (for the examples presented here, the uncertainty is of the order of 30%, Fig.24).

- The ice extent results of the icier RCO version are close to results of the Helsinki ice model by Haapala et al. (2000). However, simulated changes of mean maximum ice extent are somewhat different in the two models (100 and $144 \times 10^9 \, m^2$ for HIM and RCO-b, respectively). Thus, the sensitivity of the models on simulated climate change is different.

- The mean Baltic sea level and sea level extremes increase approximately by the same amount as the global mean sea level. However, in the Bay of Bothnia an additional increase of mean maximum annual SSH of about 26% is calculated.

Further investigations of the salinity spin-up issue are necessary performing coupled atmosphere-ocean secular transient runs.

Acknowledgments

Appendix A: Bulk formulae in case of open water

Wind stress is parameterized according to Large and Pond (1981):

$$\vec{\tau} = c_{aw}^{d}\, \rho_a \left|\vec{U}_{10}\right| \vec{U}_{10} \tag{1}$$

with

$$c_{aw}^{d} \times 10^3 = \left\{ \begin{array}{lll} 1.2 & : & 0 < \left|\vec{U}_{10}\right| \leq 11\,m/s \\ 0.49 + 0.065\left|\vec{U}_{10}\right| & : & 11 < \left|\vec{U}_{10}\right| \leq 22\,m/s \end{array} \right. \tag{2}$$

$\vec{U}_{10}$ denotes wind speed in $10\,m$ height and ρ_a air density.

The shortwave energy flux through the open water surface is

$$Q_{SW} = Q_{SW}^{0}\left(1 - \alpha_w\right) \tag{3}$$

with incoming solar radiation Q_{SW}^{0} and sea surface albedo α_w which is calculated from Fresnel's formula. According to Bodin (1979) Q_{SW}^{0} can be calculated from

$$Q_{SW}^{0} = T_u\, S_0\, \cos\theta\,(T_r - A_w)(1 - C_a\, F_a) \tag{4}$$

with the atmospherical turbidity $T_u = 0.95$, the solar constant $S_0 = 1.368 \cdot 10^3\, J\, m^{-2}\, s^{-1}$, the zenith angle θ and total cloudiness C_a. T_r and A_w are transmission and absorption functions and F_a is a cloud function:

$$T_r = 1.041 - 0.16\,\cos\theta^{-0.5} \tag{5}$$

$$F_a = 0.55 + 0.01\,\cos\theta^{-1} \tag{6}$$

$$A_w = 0.077\, m^{0.3}\,\cos\theta^{-0.3}, \tag{7}$$

with the optical path length m. The daily cycle is included in the model.

Sensible and latent heat fluxes are parameterized according to Large and Pond (1982). The sensible heat flux Q_S is given by

$$Q_S = \rho_a\, c_{pa}\, c_{aw}^{s} \left|\vec{U}_{10}\right|(T_a - T_w) \tag{8}$$

with specific heat capacity of air c_{pa}, air temperature in 2 m height T_a and water temperature of the first model layer T_w. The transfer coefficient c_{aw}^{s} (Stanton number) is given by

$$c_{aw}^{s} \times 10^3 = \left\{ \begin{array}{lll} 1.13 & : & (T_a - T_w) < 0 \quad \text{unstable} \\ 0.66 & : & (T_a - T_w) \geq 0 \quad \text{stable} \end{array} \right. \tag{9}$$

The latent heat flux Q_L is determined by

$$Q_L = L_{aw}\, E \tag{10}$$

with L_{aw} latent heat of vaporization. Evaporation E is calculated according to

$$E = \rho_a\, c_{aw}^{l} \left|\vec{U}_{10}\right|(q_a - q_w) \tag{11}$$

with q_a and q_w specific humidity in $2\,m$ height of the atmosphere and close to the water surface, respectively. $c_{aw}^l = 1.15$ is the corresponding transfer coefficient (Dalton number).

The longwave incoming ($Q_{LW\downarrow}$) and outgoing radiation ($Q_{LW\uparrow}$) are calculated according to Maykut and Church (1973) and from Stefan Boltzmann's law, respectively:

$$Q_{LW\downarrow} - Q_{LW\uparrow} = \sigma_s\, a_1\, (1 + a_2\, C_a^{2.75})\, T_a^4 - \sigma_s\, T_w^4 \tag{12}$$

with Stefan Boltzmann's constant σ_s and the empirical constants $a_1 = 0.7829$ and $a_2 = 0.2232$.

The total heat flux through the sea surface Q_a is then given by the sum

$$Q_a = Q_{SW} + Q_{LW\downarrow} - Q_{LW\uparrow} + Q_S + Q_L. \tag{13}$$

The salt flux S_F is given to

$$S_F = -(P - E)\, S \tag{14}$$

with precipitation P and salinity S of the uppermost ocean box.

Appendix B: Bulk formulae in case of sea ice

Wind stress to the ice is parameterized as in case of open water. The flux of momentum between sea ice of concentration A and the ocean is given by

$$\vec{\tau} = (1 - A)\,\vec{\tau}|_{noice} + A\,\rho_w\,c_{wi}^d\,|\vec{u}_i - \vec{u}_w|\,(\vec{u}_i - \vec{u}_w) \tag{15}$$

with the ice-ocean drag coefficient $c_{wi}^d = 3.5 \cdot 10^{-3}$, water density ρ_w, ice velocity $\vec{u}_i$ and current velocity $\vec{u}_w$.

The bulk formulae of Appendix A are used for the ice case as well with only minor changes:

In Eq.(3) ice or snow albedo $\alpha_{(i,s)}$ is used instead of sea surface albedo and in Eq.(4) the cloud cover correction of Laevastu (1960) is utilized. One fraction of the incoming solar radiation penetrates the ice heating the ocean (cf. Sahlberg 1988):

$$Q_{SW}^{ib} = \begin{cases} Q_{SW}^0\,(1 - \alpha_s)\,f_{sol}\,e^{-\kappa_s h_s - \kappa_i h_i} & \text{if } h_s > 10\ cm\,, \\[2mm] Q_{SW}^0\,(1 - \alpha_s)\,f_{sol}\,e^{-\kappa_i h_i} & \text{if } 0 < h_s \leq 10\ cm\,, \\[2mm] Q_{SW}^0\,(1 - \alpha_i)\,f_{sol}\,e^{-\kappa_i h_i} & \text{if } h_s = 0\,. \end{cases} \tag{16}$$

$\kappa_i = 1.5\,m^{-1}$ and $\kappa_s = 15\,m^{-1}$ are bulk extinction coefficients and $f_{sol} = 0.1$ a penetration factor. h_i and h_s are ice and snow thickness, respectively.

The latent heat flux over sea ice is calculated using latent heat of sublimation instead of vaporization. In all formulae the prognostic variable for ice or snow surface temperature is used instead of sea surface temperature.

The total atmosphere-ocean heat flux is given by

$$Q_a = Q_a|_{noice}(1 - A) + Q_{bottom}\,A\,. \tag{17}$$

Q_{bottom} is the heat flux between ice and ocean:

$$Q_{bottom} = \rho_w\,c_{pw}\,c_{wi}^h\,|\vec{u}_w - \vec{u}_i|\,(T_w - T_{fp}) \tag{18}$$

where c_{pw} is the specific heat of sea water and c_{wi}^h the bulk heat transfer coefficient. T_{fp} is the salinity (S) dependent, freezing point temperature according to Millero (1978)

$$T_{fp} = -0.0575\,S + 1.710523 \cdot 10^{-3}\,S^{3/2} - 2.154996 \cdot 10^{-4}\,S^2\,. \tag{19}$$

Omstedt and Wettlaufer (1992) suggested to use $c_{wi}^h = 2.8 \cdot 10^{-4}$ in order to get reasonable results. Velocity differences in Eq.(18) have to be limited to ensure minimal heat flux under fast ice (Haapala and Leppäranta 1996): $\Delta u_{min} = 0.001\ ms^{-1}$.

During the freezing process brine is released into the ocean. The total atmosphere-ocean freshwater flux is summarized in:

$$S_F = S_F|_{noice}\,(1 - A) + \frac{V_{new}}{\Delta t_e}\,\frac{\rho_i}{\rho_w}\,S \tag{20}$$

with Δt_e timestep of the ice model, ρ_i sea ice density and V_{new} volume per unit area of new ice (see Meier et al. 1999).
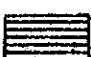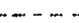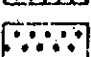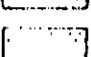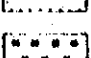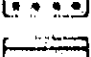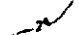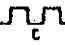
Appendix C: Ice chart key

ISLÄGE & YTVATTENTEMPERATURER

ICE CONDITION & SEA SURFACE TEMPERATURES

NR 22   1984-03-19

SYMBOLS

▨	**Fast is** / *Fast ice*	▼▼	**Stampvall** / *Windrow, Jammed brash barrier*
▦	**Sammanfrusen, kompakt eller mycket tät drivis** / *Consolidated, compact or very close ice (9–10/10)*	——	**Iskant eller isgräns** / *Ice edge or ice boundary*
▤	**Tät drivis** / *Close ice (7–8/10)*	– – –	**Uppskattad iskant eller isgräns** / *Estimated ice edge or ice boundary*
▥	**Spridd drivis** / *Open ice (4–6/10)*	⌇	**Råk** / *Lead*
⸬	**Mycket spridd drivis** / *Very open ice (1–3/10)*	⌇	**Spricka** / *Crack*
▢	**Öppet vatten** / *Open water (<1/10)*	[ɪ]	**Uppmätt istjocklek** / *Thickness measured in cm*
⸭	**Nyis** / *New ice*	△	**Isbumlingar** / *Floebergs/Floebits*
▤	**Jämn is** / *Level ice*	⌇	**Vattentemperatur isoterm i °C** / *Watertemperature isoterm, °C*
▲▲c	**Vallar och upptornad is** / *Ridged or hummocked ice (C = concentration)*	W	**Varm maximum** / *Warm maximum*
⊓⊓c	**Hopskjuten is** / *Rafted ice (C = concentration)*	C	**Kallt minimum** / *Cold minimum*

		S		F	
C = Koncentration i tiondelar / *Concentration in tenth*		**Code**	**cm**	**Code**	**ө m**
		0	–	0	<3
S = istjocklek / *Stage of development*		1	nuw ice	1	<2
		2	<10	2	<20
		3	10–30	3	20–100
F = Form av is/flakitoriek / *Form of ice/floesize*		4	10–15	4	100–500
		5	15–30	5	500–2000
		6	30–200	6	2000–10000
		7	30–70	7	<10000
		f	30–50	8	Fast ice
		9	50–70	X	unknown
		1.	70–120		
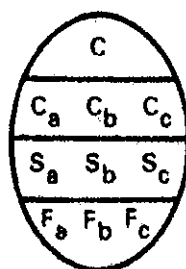
Figure 27: *Ice condition and sea surface temperatures. Magnified key of Fig.13, Fig.14 and Fig.15.*

References

Bergström S, Carlsson B (1994) River runoff to the Baltic Sea: 1950-1990. Ambio 23:280-287

Bodin S (1979) A predictive numerical model of the atmospheric boundary layer based on the turbulent energy equation. Report Meteorology and Climatology No. 13, Swedish Meteorological and Hydrological Institute, SE-60176 Norrköping, Sweden, 139 pp

Bryan K (1969) A numerical method for the study of the circulation of the World Ocean. J Comput Phys 4:347-376

Bryan K, Cox MD (1972) An approximate equation of state for numerical models of ocean circulation. J Phys Oceanogr 2:510-514

Bumke K, Karger U, Hasse L, Niekamp K (1998) Evaporation over the Baltic Sea as an example of a semi-enclosed sea. Contr Atmos Phys 71:249-261

Cox MD (1984) A primitive equation 3-dimensional model of the ocean. GFDL Ocean Group Tech Rep No. 1, GFDL, Princeton University, U.S.A.

Ekman M (1996) A consistent map of the postglacial uplift of Fennoscandia. Terra Nova 8:158-165

Ekman M (1999) Climate changes detected through the world's longest sea level series. Global and Planetary Change 21:215-224

Ekman M, Mäkinen J (1996) Mean sea surface topography in the Baltic sea and its transition area to the North Sea: A geodetic solution and comparison with oceanographic models. J Geophys Res 101:11993-11999

Finnish Marine Research (anonymous) (1982) Ice winters 1976-1980 along the Finnish coast. Finnish Marine Research 249:46

Gibson JK, Kållberg P, Uppala S, Hernandez A, Nomura A, Serrano E (1997) ERA description. ECMWF Re-analysis Project Rep. Series 1, European Centre for Medium-Range Weather Forecasts, Reading, United Kingdom, 66 pp

Gill AE (1982) Atmosphere-ocean dynamics. Academic Press, London, 662 pp

Graham PL (1999) Modeling runoff to the Baltic Sea. Ambio 27:328-334

Haapala J (2000) On the modelling of ice thickness redistribution. J. Glaciology, in press

Haapala J, Leppäranta M (1996) Simulating the Baltic Sea ice season with a coupled ice-ocean model. Tellus 48A:622-643

Haapala J, Leppäranta M (1997) The Baltic Sea ice season in changing climate. Boreal Environ Res 2:93-108

Haapala J, Alenius P, Dubra J, Klyachkin SV, Kouts T, Leppäranta M, Omstedt A, Pakstys L, Schmelzer N, Schrum C, Seinä A, Strübing K, Sztobryn M, Zaharchenko E (1996) IDA - Ice data bank for Baltic Sea climate studies. Report series in Geophysics No.35, University of Helsinki, 45pp

Haapala J, Juottonen A, Marnela M, Leppäranta M, Tuomenvirta H (2000) Modelling the variability of the sea ice conditions in the Baltic Sea under different climate conditions. Annals of Glaciology, accepted

Hibler WD (1979) A dynamic thermodynamic sea ice model. J Phys Oceanogr 9:817-846

Hilmer M, Jung T (2000) Evidence for a recent change in the link between the North Atlantic Oscillation and Arctic sea ice export. Geophys Res Lett 27:989-992

Hulme M, Conway D, Jones PD, Jiang T, Zhou X, Barrow EM, Turney C (1995) A 1961-90 gridded surface climatology for Europe, 51 pp + maps (available from Climatic Research Unit, Norwich)

Hunke EC, Dukowicz JK (1997) An elastic-viscous-plastic model for sea ice dynamics. J Phys Oceanogr 27:1849-1867

Hunke EC, Zhang Y (1999) A Comparison of Sea Ice Dynamics Models at High Resolution, Mon Wea Rev 127:396-408

Johns TC, Carnell RE, Crossley JF, Gregory JM, Mitchell JFB, Senior CA, Tett SFB, Wood RA (1997) The second Hadley Centre coupled ocean-atmosphere GCM: Model description, spinup and validation. Clim Dyn 13:103-134

Kalliosaari S, Seinä A (1987) Ice winters 1981-85 along the Finnish coast. Finnish Marine Research 254:1-63

Kauker F (1998) Regionalization of climate model results for the North Sea. PhD thesis, University of Hamburg, Germany, 109 pp

Källén E (ed) (1996) HIRLAM documentation manual. System 2.5. Swedish Meteorological and Hydrological Institute, SE-60176 Norrköping, Sweden. 178 pp + 55 pp appendix

Killworth PD, Stainforth D, Webb DJ, Paterson SM (1991) The development of a free-surface Bryan-Cox-Semtner ocean model. J Phys Oceanogr 21:1333-1348

Knudsen M (1899) The hydrographic conditions in the Danish waters inside Skagen in 1894-98 (in Danish). Komm For Vidensk Unders I de danske farvande 2:2

Knudsen M (1900) A hydrographical theorem (in German). Ann Hydr 28:316-320

Koslowski G, Loewe P (1994) The western Baltic sea ice season in terms of mass-related severity index: 1879-1992. Part I. Temporal variability and association with the north Atlantic oscillation. Tellus 46A:66-74

Laevastu T (1960) Factors affecting the temperature of the surface layer of the sea. Commentat Phys Math 25:8-134

Large WG, Pond S (1981) Open ocean momentum flux measurements in moderate to strong winds. J Phys Oceanogr 11:324-336

Large WG, Pond S (1982) Sensible and latent heat flux measurements over the ocean. J Phys Oceanogr 12:464-482

Lass HU, Matthäus W (1996) On temporal wind variations forcing salt water inflows into the Baltic Sea. Tellus 48A:663-671

Ljungemyr P, Gustafsson N, Omstedt A (1996) Parameterization of lake thermodynamics in a high resolution weather forecasting model. Tellus 48A:608-621

Matthäus W, Franck H (1992) Characteristics of major Baltic inflows - a statistical analysis. Cont Shelf Res 12:1375-1400

Matthäus W, Lass HU (1995) The recent salt inflow into the Baltic Sea. J Phys Oceanogr 25:280-286

Matthäus W, Schinke H (1994) Mean atmospheric circulation patterns associated with major Baltic inflows. Dt hydrogr Z 46:321-339

Matthäus W, Schinke H (1999) The influence of river runoff on deep water conditions of the Baltic Sea. Hydrobiologia 393:1-10

Maykut GA, Church P (1973) Radiation climate of Barrow, Alaska, 1962-1966. J Appl Meteorol 12:620-628

Meier HEM (1999) First results of multi-year simulations using a 3D Baltic Sea model. Reports Oceanography No.27, Swedish Meteorological and Hydrological Institute, SE-60176 Norrköping, Sweden, 48 pp

Meier HEM (2000) The use of the $k - \epsilon$ turbulence model within the Rossby Centre regional ocean climate model: parameterization development and results. Reports Oceanography No.28, Swedish Meteorological and Hydrological Institute, SE-60176 Norrköping, Sweden, 81 pp

Meier HEM, Faxén T (2001) Performance analysis of a multiprocessor coupled ice-ocean model for the Baltic Sea. Submitted.

Meier HEM, Döscher R, Coward AC, Nycander J, Döös K (1999) RCO - Rossby Centre regional Ocean climate model: model description (version 1.0) and first results from the hindcast period 1992/93. Reports Oceanography No.26, Swedish Meteorological and Hydrological Institute, SE-60176 Norrköping, Sweden, 102 pp

Meier HEM, Döscher R, Faxén T (2001) A multiprocessor coupled ice-ocean model for the Baltic Sea. Submitted.

Mesinger F, Arakawa A (1976) Numerical methods used in atmospheric models, Vol. 1, GARP Publications Series No.17, WMO, Geneva, 64 pp

Millero FJ (1978) Freezing point of sea water. Eigth report of the joint panel of oceanographic tables and standards, UNESCO Technical Papers in marine science No.28, Paris, France

Mitchell JFB, Johns TC (1997) On modification of global warming by sulphate aerosols. J Climate 10:245-267

Omstedt A (1990) Modelling the Baltic Sea as thirteen sub-basins with vertical resolution. Tellus 42A:286-301

Omstedt A, Nyberg L (1996) Response of Baltic Sea ice to seasonal, interannual forcing and climate change. Tellus 48A:644-662

Omstedt A, Rutgersson A (2000) Closing the water and heat cycles of the Baltic Sea. Meteorol Z 9:57-64

Omstedt A, Wettlaufer JS (1992) Ice growth and oceanic heat flux, models and measurements. J Geophys Res 97:9383-9390

Omstedt A, Gustafsson B, Rodhe J, Walin G (2000) Use of Baltic Sea modelling to investigate the water cycle and the heat balance in GCM and regional climate models. Clim Res 15:95-108

Omstedt A, Nyberg L, Meuller L (1997) Interannual, seasonal and regional variations of precipitation and evaporation over the Baltic Sea. Ambio 26:644-662

Omstedt A, Sahlberg J, Svensson U (1983) Measured and numerically-simulated autumn cooling in the Bay of Bothnia. Tellus 35A:231-240

Perovich DK (1996) The optical properties of sea ice. CRREL Monograph 96-1, Hanover, NH, U.S.A.

Rodi W (1980) Turbulence models and their application in hydraulics - a state-of-the-art review. Int Assoc for Hydraul Res, Delft, Netherlands, 104 pp

Roeckner E, Oberhuber JM, Bacher A, Christoph M, Kirchner I (1996) ENSO variability and atmospheric response in a global atmosphere-ocean GCM. Clim Dyn 12:737-754

Rummukainen M, Räisänen J, Bringfelt B, Ullerstig A, Omstedt A, Willén U, Hansson U, Jones C (2000) A regional climate model for northern Europe - model description and results from the downscaling of two GCM control simulations. Clim Dyn, in press

Räisänen J (1999) Internal variability as a cause of qualitative intermodel disagreement on anthropogenic climate change. Theor Appl Climatol 64:1-13

Räisänen J, Döscher R (1999) Simulation of present-day climate in Northern Europe in HadCM2 OAGCM. Reports Meteorology and Climatology No.84, Swedish Meteorological and Hydrological Institute, SE-60176 Norrköping, Sweden, 37 pp

Räisänen J, Rummukainen M, Ullerstig A, Bringfelt B, Hansson U, Willén U (1999) The first Rossby Centre regional climate scenario - dynamical downscaling of CO_2-induced climate change in the HadCM2 GCM. Reports Meteorology and Climatology No.85, Swedish Meteorological and Hydrological Institute, SE-60176 Norrköping, Sweden, 56 pp

Räisänen J, Rummukainen M, Ullerstig A (2000) Downscaling of greenhouse gas induced climate change in two GCM's with the Rossby Centre regional climate model for northern Europe. Tellus, in press

Saloranta TM (2000) Modeling the evolution of snow, snow ice and ice in the Baltic Sea. Tellus 52A:93-108

Sahlberg J (1988) Modelling of the thermal regime of a lake during winter season. Cold Region Science and Technology 15:151-159

Schinke H, Matthäus W (1998) On the causes of major Baltic inflows - an analysis of long time series. Cont Shelf Res 18:67-97

Schrum C, Janssen F, Hübner U (2000) Recent climate modelling in North Sea and Baltic Sea. Part A: Model description and validation. Ber. Zentrum f. Meeres- u. Klimaforschung No.37, Hamburg, Germany, 60 pp

Seifert T, Kayser B (1995) A high resolution spherical grid topography of the Baltic Sea. Meereswiss Ber Warnemünde 9:73-88

Seinä A, Kalliosaari S (1991) Ice winters 1986-1990 along the Finnish coast. Finnish Marine Research 259:3-61

Seinä A, Peltola J (1991) Duration of the ice season and statistics of fast ice thickness along the Finnish coast 1961-1990. Finnish Marine Research 258

Seinä A, Grönvall H, Kalliosaari S, Vainio J (1996) Ice season 1991-1995 along the Finnish coast. Meri, Report Series of the Finnish Institute of Marine Research 27:3-76

Semtner AJ (1974) A general circulation model for the World Ocean. Tech Rep No.9, Department of Meteorology, University of California, Los Angeles, 99 pp

Semtner AJ (1976) A model for the thermodynamic growth of sea ice in numerical investigations of climate, J Phys Oceanogr 6:379-389

Sjöberg B (ed) (1992) Sea and Coast. The National Atlas of Sweden. Almqvist and Wiksell International, Stockholm, 128 pp

SMHI, FIMR (1982) Climatological Ice Atlas for the Baltic Sea, Kattegat, Skagerrak and Lake Vänern (1963-1979). SE-60176 Norrköping, Sweden, 220 pp

Stevens DP (1990) On open boundary conditions for three dimensional primitive equation ocean circulation models. Geophys Astrophys Fluid Dynamics 51:103-133

Stevens DP (1991) The open boundary condition in the United Kingdom fine-resolution Antarctic model. J Phys Oceanogr 21:1494-1499

Svensson U (1978) A mathematical model of the seasonal thermocline. Rep. 1002, Dep. of Water Resour. Eng., Univ. of Lund, Lund, Sweden, 187 pp

Tinz B (1996) On the relation between annual maximum extent of ice cover in the Baltic Sea level pressure as well as air temperature field. Geophysica 32:319-341

UNESCO (1981) Tenth report of the joint panel on oceanographic tables and standards. UNESCO Technical Papers in Marine Sci No.36, UNESCO, Paris, France

Webb DJ (1995) The vertical advection of momentum in Bryan-Cox-Semtner Ocean General Circulation models, J Phys Oceanogr 25:3186-3195

Webb DJ, Coward AC, de Cuevas BA, Gwilliam CS (1997) A multiprocessor ocean circulation model using message passing. J Atmos Oceanic Technol 14:175-183

Webb DJ, de Cuevas BA, Richmond CS (1998) Improved advection schemes for ocean models. J Atmos Oceanic Technol 15:1171-1187

Welander P (1974) Two-layer exchange in an estuary basin, with special reference to the Baltic Sea. J Phys Oceanogr 4:542-556

List of Figures

List of Tables

62

SMHIs publications

SMHI publishes six report series. Three of these, the R-series, are intended for international readers and are in most cases written in English. For the others the Swedish language is used.

Names of the Series	Published since
RMK (Report Meteorology and Climatology)	1974
RH (Report Hydrology)	1990
RO (Report Oceanography)	1986
METEOROLOGI	1985
HYDROLOGI	1985
OCEANOGRAFI	1985

Earlier issues published in serie RMK

1   Thompson, T., Udin, I., and Omstedt, A. (1974)
     Sea surface temperatures in waters surrounding Sweden.

2   Bodin, S. (1974)
     Development on an unsteady atmospheric boundary layer model.

3   Moen, L. (1975)
     A multi-level quasi-geostrophic model for short range weather predictions.

4   Holmström, I. (1976)
     Optimization of atmospheric models.

5   Collins, W.G. (1976)
     A parameterization model for calculation of vertical fluxes of momentum due to terrain induced gravity waves.

6   Nyberg, A. (1976)
     On transport of sulphur over the North Atlantic.

7   Lundqvist, J.-E., and Udin, I. (1977)
     Ice accretion on ships with special emphasis on Baltic conditions.

8   Eriksson, B. (1977)
     Den dagliga och årliga variationen av temperatur, fuktighet och vindhastighet vid några orter i Sverige.

9   Holmström, I., and Stokes, J. (1978)
     Statistical forecasting of sea level changes in the Baltic.

10   Omstedt, A., and Sahlberg, J. (1978)
     Some results from a joint Swedish-Finnish sea ice experiment, March, 1977.

11   Haag, T. (1978)
     Byggnadsindustrins väderberoende, seminarieuppsats i företagsekonomi, B-nivå.

12   Eriksson, B. (1978)
     Vegetationsperioden i Sverige beräknad från temperaturobservationer.

13   Bodin, S. (1979)
     En numerisk prognosmodell för det atmosfäriska gränsskiktet, grundad på den turbulenta energiekvationen.

14   Eriksson, B. (1979)
     Temperaturfluktuationer under senaste 100 åren.

15 Udin, I., och Mattisson, I. (1979)
Havsis- och snöinformation ur datorbear-
betade satellitdata - en modellstudie.

16 Eriksson, B. (1979)
Statistisk analys av nederbördsdata. Del I.
Arealnederbörd.

17 Eriksson, B. (1980)
Statistisk analys av nederbördsdata. Del II.
Frekvensanalys av månadsnederbörd.

18 Eriksson, B. (1980)
Årsmedelvärden (1931-60) av nederbörd, av-
dunstning och avrinning.

19 Omstedt, A. (1980)
A sensitivity analysis of steady, free floating
ice.

20 Persson, C., och Omstedt, G. (1980)
En modell för beräkning av luftföroreningars
spridning och deposition på mesoskala.

21 Jansson, D. (1980)
Studier av temperaturinversioner och vertikal
vindskjuvning vid Sundsvall-Härnösands
flygplats.

22 Sahlberg, J., and Törnevik, H. (1980)
A study of large scale cooling in the Bay of
Bothnia.

23 Ericson, K., and Hårsmar, P.-O. (1980)
Boundary layer measurements at Klock-rike.
Oct. 1977.

24 Bringfelt, B. (1980)
A comparison of forest evapotranspiration
determined by some independent methods.

25 Bodin, S., and Fredriksson, U. (1980)
Uncertainty in wind forecasting for wind po-
wer networks.

26 Eriksson, B. (1980)
Graddagsstatistik för Sverige.

27 Eriksson, B.(1981)
Statistisk analys av nederbördsdata. Del III.
200-åriga nederbördsserier.

28 Eriksson, B. (1981)
Den "potentiella" evapotranspirationen i
Sverige.

29 Pershagen, H. (1981)
Maximisnödjup i Sverige (perioden
1905-70).

30 Lönnqvist, O. (1981)
Nederbördsstatistik med praktiska tillämp-
ningar.
(Precipitation statistics with practical appli-
cations.)

31 Melgarejo, J.W. (1981)
Similarity theory and resistance laws for the
atmospheric boundary layer.

32 Liljas, E. (1981)
Analys av moln och nederbörd genom
automatisk klassning av AVHRR-data.

33 Ericson, K. (1982)
Atmospheric boundary layer field experiment
in Sweden 1980, GOTEX II, part I.

34 Schoeffler, P. (1982)
Dissipation, dispersion and stability of
numerical schemes for advection and dif-
fusion.

35 Undén, P. (1982)
The Swedish Limited Area Model. Part A.
Formulation.

36 Bringfelt, B. (1982)
A forest evapotranspiration model using sy-
noptic data.

37 Omstedt, G. (1982)
Spridning av luftförorening från skorsten i
konvektiva gränsskikt.

38 Törnevik, H. (1982)
An aerobiological model for operational
forecasts of pollen concentration in the air.

39 Eriksson, B. (1982)
Data rörande Sveriges temperaturklimat.

40 Omstedt, G. (1984)
An operational air pollution model using
routine meteorological data.

41 Persson, C., and Funkquist, L. (1984)
Local scale plume model for nitrogen
oxides. Model description.

42 Gollvik, S. (1984)
Estimation of orographic precipitation by dy-
namical interpretation of synoptic model
data.

43 Lönnqvist, O. (1984)
Congression - A fast regression technique
with a great number of functions of all pre-
dictors.

44 Laurin, S. (1984)
Population exposure to SO and NO_x from
different sources in Stockholm.

45 Svensson, J. (1985)
Remote sensing of atmospheric tempera-ture
profiles by TIROS Operational Vertical
Sounder.

46 Eriksson, B. (1986)
Nederbörds- och humiditetsklimat i
Sverige under vegetationsperioden.

47 Taesler, R. (1986)
Köldperioden av olika längd och förekomst.

48 Wu Zengmao (1986)
Numerical study of lake-land breeze over
Lake Vättern, Sweden.

49 Wu Zengmao (1986)
Numerical analysis of initialization
procedure in a two-dimensional lake
breeze model.

50 Persson, C. (1986)
Local scale plume model for nitrogen
oxides. Verification.

51 Melgarejo, J.W. (1986)
An analytical model of the boundary layer
above sloping terrain with an application to
observations in Antarctica.

52 Bringfelt, B. (1986)
Test of a forest evapotranspiration model.

53 Josefsson, W. (1986)
Solar ultraviolet radiation in Sweden.

54 Dahlström, B. (1986)
Determination of areal precipitation for the
Baltic Sea.

55 Persson, C. (SMHI), Rodhe, H. (MISU), De
Geer, L.-E. (FOA) (1986)
The Chernobyl accident - A meteorological
analysis of how radionucleides reached
Sweden.

56 Persson, C., Robertson, L. (SMHI), Grenn-
felt, P., Kindbom, K., Lövblad, G., och
Svanberg, P.-A. (IVL) (1987)
Luftföroreningsepisoden över södra
Sverige 2 - 4 februari 1987.

57 Omstedt, G. (1988)
An operational air pollution model.

58 Alexandersson, H., Eriksson, B. (1989)
Climate fluctuations in Sweden
1860 - 1987.

59 Eriksson, B. (1989)
Snödjupsförhållanden i Sverige -
Säsongerna 1950/51 - 1979/80.

60 Omstedt, G., Szegö, J. (1990)
Människors exponering för luftföroreningar.

61 Mueller, L., Robertson, L., Andersson, E.,
Gustafsson, N. (1990)
Meso-γ scale objective analysis of near surfa-
ce temperature, humidity and wind, and its
application in air pollution modelling.

62 Andersson, T., Mattisson, I. (1991)
A field test of thermometer screens.

63 Alexandersson, H., Gollvik, S.,
Meuller, L. (1991)
An energy balance model for prediction of
surface temperatures.

64 Alexandersson, H., Dahlström, B. (1992)
Future climate in the Nordic region -
survey and synthesis for the next century.

65 Persson, C., Langner, J., Robertson, L.
(1994)
Regional spridningsmodell för Göteborgs
och Bohus, Hallands och Älvsborgs län. (A
mesoscale air pollution dispersion model for
the Swedish west-coast region. In Swedish
with captions also in English.)

66 Karlsson, K.-G. (1994)
Satellite-estimated cloudiness from NOAA
AVHRR data in the Nordic area during 1993.

67   Karlsson, K-G. (1996)
      Cloud classifications with the SCANDIA
      model.

68   Persson, C., Ullerstig, A. (1996)
      Model calculations of dispersion of lindane
      over Europe. Pilot study with comparisons to
      measurements around the Baltic Sea and the
      Kattegat.

69   Langner, J., Persson, C., Robertson, L., and
      Ullerstig, A. (1996)
      Air pollution Assessment Study Using the
      MATCH Modelling System. Application to
      sulfur and nitrogen compounds over Sweden
      1994.

70   Robertson, L., Langner, J., Engardt, M.
      (1996)
      MATCH - Meso-scale Atmosperic Transport
      and Chemistry modelling system.

71   Josefsson, W. (1996)
      Five years of solar UV-radiation monitoring
      in Sweden.

72   Persson, C., Ullerstig, A., Robertson, L.,
      Kindbom, K., Sjöberg, K. (1996)
      The Swedish Precipitation Chemistry
      Network. Studies in network design using the
      MATCH modelling system and statistical
      methods.

73   Robertson, L. (1996)
      Modelling of anthropogenic sulfur deposition
      to the African and South American
      continents.

74   Josefsson, W. (1996)
      Solar UV-radiation monitoring 1996.

75   Häggmark, L., Ivarsson, K.-I. (SMHI),
      Olofsson, P.-O. (Militära vädertjänsten).
      (1997)
      MESAN - Mesoskalig analys.

76   Bringfelt, B, Backström, H, Kindell, S,
      Omstedt, G, Persson, C, Ullerstig, A. (1997)
      Calculations of PM-10 concentrations in
      Swedish cities- Modelling of inhalable
      particles

77   Gollvik, S. (1997)
      The Teleflood project, estimation of
      precipitation over drainage basins.

78   Persson, C., Ullerstig, A. (1997)
      Regional luftmiljöanalys för Västmanlands
      län baserad på MATCH modell-beräkningar
      och mätdata - Analys av 1994 års data

79   Josefsson, W., Karlsson, J.-E. (1997)
      Measurements of total ozone 1994-1996.

80   Rummukainen, M. (1997)
      Methods for statistical downscaling of GCM
      simulations.

81   Persson, T. (1997)
      Solar irradiance modelling using satellite
      retrieved cloudiness - A pilot study

82   Langner, J., Bergström, R. (SMHI) and
      Pleijel, K. (IVL) (1998)
      European scale modelling of sulfur, oxidized
      nitrogen and photochemical oxidants. Model
      development and evaluation for the 1994
      growing season.

83   Rummukainen, M., Räisänen, J., Ullerstig,
      A., Bringfelt, B., Hansson, U., Graham, P.,
      Willén, U. (1998)
      RCA - Rossby Centre regional Atmospheric
      climate model: model description and results
      from the first multi-year simulation.

84   Räisänen, J., Döscher, R. (1998)
      Simulation of present-day climate in Northen
      Europé in the HadCM2 OAGCM.

85   Räisänen, J., Rummukainen, M.,
      Ullerstig, A., Bringfelt, B., Ulf Hansson, U.,
      Willén, U. (1999)
      The First Rossby Centre Regional Climate
      Scenario - Dynamical Downscaling of CO_2-
      induced Climate Change in the HadCM2
      GCM.

86   Rummukainen, Markku. (1999)
      On the Climate Change debate

87   Räisänen, Jouni (2000)
      CO_2-induced climate change in northern
      Europé: comparison of 12 CMIP2
      experiments.

88   Engardt, Magnuz (2000)
      Sulphur simulations for East Asia using the
      MATCH model with meteorological data
      from ECMWF.

89   Persson, Thomas (2000)
     Measurements of Solar Radiation in Sweden
     1983-1998

90   Daniel B. Michelson, Tage Andersson
     Swedish Meteorological and Hydrological
     Institute (2000)
     Jarmo Koistinen, Finnish Meteorological
     Institute
     Christopher G. Collier, Telford Institute of
     Environmental Systems, University of
     Salford
     Johann Riedl, German Weather Service
     Jan Szturc, Instiute of Meteorology and
     Water Management
     Uta Gjertsen, The Norwegian Meteorological
     Institute
     Aage Nielsen, Danish Meteorological
     Institute
     Søren Overgaard, Danish Meteorological
     Institute
     BALTEX Radar Data Centre Products and
     their Methodologies

91   Josefsson, Weine (2000)
     Measurements of total ozone 1997 – 1999

92   Andersson, Tage (2000)
     Boundary clear air echos in southern Sweden

93   Andersson, Tage (2000)
     Using the Sun to check some weather radar
     parameters

94   Rummukainen, M., S. Bergström, E. Källén,
     L. Moen, J. Rodhe (2000)
     SWECLIM – The First Three Years

.